eNeuro

Research Article: New Research | Cognition and Behavior

Reward devaluation attenuates cue-evoked sucrose seeking and is associated with the elimination of excitability differences between ensemble and non-ensemble neurons in the nucleus accumbens

https://doi.org/10.1523/ENEURO.0338-19.2019

Cite as: eNeuro 2019; 10.1523/ENEURO.0338-19.2019

Received: 14 June 2019
Revised: 10 July 2019
Accepted: 14 July 2019

Manuscript Title Page

1. Manuscript Title:
Reward devaluation attenuates cue-evoked sucrose seeking and is associated with the elimination of excitability differences between ensemble and non-ensemble neurons in the nucleus accumbens

2. Abbreviated Title: Devaluation modulates accumbens excitability

3. List all Author Names and Affiliations:
Meike C. Sieburg[1,2], Joseph J. Ziminski[1], Gabriella Margetts-Smith[1,3], Hayley Reeve[1], Leonie S. Brebner[1], Hans S. Crombag[1], Eisuke Koya[1]
[1]Sussex Neuroscience, School of Psychology, University of Sussex, Falmer, BN1 9QG, United Kingdom.

4. Author Contributions:
MCS, GMS, HSC, EK designed research; MCS, JJZ, GMS, HR, LSB performed research; MCS, JJZ, GMS analyzed data; MCS, JJZ, HSC, EK wrote the paper.

5. Correspondence should be addressed to:
Dr. Eisuke Koya, Sussex Neuroscience, School of Psychology, University of Sussex, Falmer, BN1 9QG, United Kingdom, Tel: +44-1273-877-776, E-mail: e.koya@sussex.ac.uk

6. Number of Figures: 5

7. Number of Tables: 1

8. Number of Multimedia: 0

9. Number of words for Abstract: 250

10. Number of words for Significance Statement: 114

11. Number of words for Introduction: 592

12. Number of words for Discussion: 2,241

13. Acknowledgements:
We thank Yavin Shaham (NIDA IRP, USA) for providing helpful advice regarding the devaluation experiments.
[2]Current address: Department of Biomedicine/DANDRITE, Aarhus University, 8000 Aarhus C, Denmark
[3]Current address: University of Exeter College of Medicine and Health, Hatherly Laboratories, Prince of Wales Road, Exeter EX4 4PS, United Kingdom.

14. Conflict of Interest: Authors report no conflict of interest

15. Funding sources:
This research was supported by the Biotechnology and Biological Sciences Research Council (BBSRC) grant number BB/M009017/1; and The University of Sussex Strategic Development Funds, Sussex Neuroscience 4-year PhD programme.

Abstract

Animals must learn relationships between foods and the environmental cues that predict their availability for survival. Such cue-food associations are encoded in sparse sets of neurons or 'neuronal ensembles' in the nucleus accumbens (NAc). For these ensemble-encoded, cue-controlled appetitive responses to remain adaptive, they must allow for their dynamic updating depending on acute changes in internal states such as physiological hunger or the perceived desirability of food. However, how these neuronal ensembles are recruited and physiologically modified following the update of such learned associations is unclear. To investigate this, we examined the effects of devaluation on ensemble plasticity at the levels of recruitment, intrinsic excitability, and synaptic physiology in sucrose conditioned *Fos-GFP* mice that express green fluorescent protein (GFP) in recently activated neurons. Neuronal ensemble activation patterns and their physiology were examined using immunohistochemistry and slice electrophysiology, respectively. Reward-specific devaluation following four days of *ad lib* sucrose consumption, but not general caloric devaluation, attenuated cue-evoked sucrose seeking. This suggests that changes in the hedonic and/or incentive value of sucrose, and not caloric need drove this behavior. Moreover, devaluation attenuated the size of the neuronal ensemble recruited by the cue in the NAc shell. Finally, it eliminated the relative enhanced excitability of ensemble (GFP+) neurons against non-ensemble (GFP–) neurons observed under Non-devalued conditions, and did not induce any ensemble-specific changes in excitatory synaptic physiology. Our findings provide new insights into neuronal ensemble mechanisms that underlie the changes in the incentive and/or hedonic impact of cues that support adaptive food seeking.

Significance statement

Learned associations between food and the cues that predict their availability are encoded in neuronal ensembles in reward-relevant brain areas, such as the nucleus accumbens. Such learning is often accompanied by synaptic and intrinsic plasticity within these ensemble neurons. However, it is unclear how these plasticity changes manifest specifically in cue-activated neurons in response to decreases in reward value, e.g. following reward-specific or general (caloric) devaluation. We reveal that shifts in excitability, but not excitatory synaptic physiology between ensemble and non-ensemble neurons in the nucleus accumbens shell coincide with reward-specific devaluation. Our findings provide new insights into how changes in the perceived properties of food reward update cue-food associations by potentially fine-tuning neuronal excitability.

Introduction

Animals and humans form associations between environmental cues and the foods whose availability they predict (Jansen et al., 2016; Petrovich, 2013). Such cues obtain motivational significance following Pavlovian conditioning and exert powerful control over food seeking (Day & Carelli, 2007; Petrovich, 2013). Critically, organisms have to adapt their appetitive behaviors and related physiological responses not only according to the changing external, but also internal environment. For instance, excessive consumption of a certain type of food can alter its current attractiveness via changes in homeostatic need or its incentive and/or hedonic properties to regulate cue-responsivity (Goldstone et al., 2009; Holland & Rescorla, 1975; West & Carelli, 2016). The malfunctioning of such behavioral flexibility may lead to inappropriate responding to food cues and dysregulation of food intake (i.e. overeating), and contribute to excessive weight gain (Boswell & Kober, 2016; Jones et al., 2018; Kosheleff et al., 2018). These are pressing issues in today's society, in which we are surrounded by cues associated with unhealthy foods (e.g. junk food advertisements). Hence, elucidating the neurobiological processes underlying the updating of cue-food associations is crucial to obtain a better understanding of maladaptive eating behaviors.

It has been shown that associations between cues and rewarding substances such as food and drugs of abuse are dependent on sparsely distributed sets of neurons called neuronal ensembles (Pennartz et al., 1994; Carelli et al., 2000; Koya et al., 2009a; Whitaker et al., 2016, 2017; Ziminski et al., 2017, 2018). These neurons can act as memory engrams to encode and store cue-reward memory representations (Tonegawa et al., 2015; Whitaker & Hope, 2018). In addition to other mesocorticolimbic structures, these appetitive memory ensembles are found in the nucleus accumbens (NAc); a brain area well-established to play a causal role in hedonic processing and incentive learning (Castro et al., 2015; Day & Carelli, 2007; Kelley, 2004; West & Carelli, 2016).

123 Importantly, intrinsic and synaptic plasticity modulate neuronal network function in the wider
124 mesocorticolimbic network and plays a pivotal role in many forms of associative learning
125 (Kourrich et al., 2015; Stuber et al., 2008; Whitaker et al., 2017). The former primarily
126 involves changes in the neuron's electrical or excitability properties that influence neuronal
127 firing, while the latter involves changes in neuronal communication at the synapse (Kourrich
128 et al., 2015). For instance, studies using *Fos-GFP* mice that express GFP in behaviorally
129 activated neurons have shown that intrinsic and synaptic plasticity within NAc ensembles,
130 particularly in the shell region, help to encode cue-reward associations (Barth, 2004;
131 Whitaker et al., 2016; Ziminski et al., 2017). Recently, it was found that changes in appetitive
132 associative strength following extinction learning restricted the ability of food cues to recruit a
133 hyperexcitable neuronal ensemble in the NAc shell subregion (Ziminski et al., 2017). Also,
134 studies have shown that NAc shell neurons activated by specific drug-cue associations
135 exhibit remodeling of excitatory glutamatergic synapses (Koya et al., 2012; Whitaker et al.,
136 2016). Taken together, physiological modifications in a select group of neurons are likely to
137 establish highly specific appetitive associative memories.

138

139 Here, we examined how ensemble-specific changes in intrinsic and synaptic plasticity
140 underlie updating of cue-food associations using a reward-specific devaluation procedure.
141 This approach is widely used to assess behavioral flexibility following changes in the
142 rewarding value of food (West & Carelli, 2016). To this end, we devalued sucrose reward
143 using a reward-specific, sucrose satiation procedure and compared it to a non-reward
144 specific satiation manipulation. Subsequently, we examined plasticity changes in
145 behaviorally activated NAc shell neurons in sucrose conditioned *Fos-GFP* mice at the levels
146 of ensemble size, excitability, and synaptic physiology following reward-specific devaluation.

147

Material and Methods

Animals

Male wild-type C57BL/6 mice were purchased from Charles River UK. Male heterozygous *Fos-GFP* mice (https://www.jax.org/strain/014135, RRID:IMSR_JAX:014135) on a C57BL/6 background that originated from the laboratory of Allison Barth (Carnegie Mellon University) were obtained from the in-house breeding programme at the University of Sussex (UK). All mice were housed 2-3 per cage and maintained on a 12:12 hour light/dark cycle (lights on at 7:00) at a temperature of 21±1 °C and 50±5% humidity, and had access to standard chow (BK001 E Rodent Breeder and Grower diet, SDS) and *ad libitum (ad lib)* water. Unless noted, one week prior to and for the entire duration of the behavioral experiments, mice were food restricted to 90% of their free-feeding body weight (adjusted for age). Mice were 9-10 weeks old at the beginning of behavioral testing. *Fos-GFP* mice were used for experiments examining the effects of devaluation on Pavlovian approach (cue-evoked food seeking), Fos expression, and physiological parameters. These mice condition and exhibit food seeking similarly to wild-type mice *(Ziminski et al., 2017)*. Wild-type mice were used for the experiments examining the effects of caloric satiation on Pavlovian approach. All experiments were conducted during the light phase. All animal procedures were performed in accordance with the University of Sussex animal care committee's regulations.

Behavioral experiments

Apparatus

All behavioral procedures were carried out in conditioning chambers (15.9 x 14 x 12.7 cm, Med Associates, Vermont, USA) each enclosed within a sound attenuating and light resistant cubicle. The conditioning chamber was fitted with a recessed magazine situated in the center of one side-wall which dispensed 10 % sucrose solution serving as the

unconditioned stimulus (US). An infrared beam detected head entries into the magazine. The house light was situated in the side panel and was on for the duration of each training or test session. A mechanical relay served as an auditory (click) conditioned stimulus (CS) (Med Associates). Initiation and running of behavioral protocols, including the recording of head entries into the food magazine, was performed using Med-PC IV (MedAssociates Inc., RRID:SCR_012156).

Behavioral procedures

Prior to conditioning, mice underwent a single session of magazine training, which began following the initial head entry into the food magazine. During this session they received 40 presentations of 10% sucrose solution (~15 µl) in the food magazine on a random interval 30 (RI30) schedule in order to get accustomed to the sucrose delivery procedure. Starting the next day, mice underwent 11-12 Pavlovian conditioning sessions (on average 24 minutes per session; 1-2 times daily in the morning (8 am-12 noon) and/or afternoon (12 noon-5 pm) over 7 consecutive days. The illumination of the house light indicated the start of each session, which consisted of six 120 s CS presentations (yoked across conditioning chambers), separated by 120 s RI intertrial interval (ITI) periods. During each 120 s CS period, ~15 µL of 10% sucrose solution was delivered into the magazine on a RI-30 s schedule. Following conditioning, mice remained in the colony room for 7-9 days until test day. Three days following the final conditioning session (Figure 1A), mice were randomly allocated to one of two groups for the remaining 4-6 days for: 1) Reward-specific devaluation experiments in which all mice continued to be food restricted, and one group of mice (Devalued group) received *ad lib* sucrose solution in their home cage whereas the control (Non-devalued) group received an additional water bottle; 2) caloric satiation experiments in which one group of mice (*ad lib* chow group) received *ad lib* chow in their home cage whereas the Control group continued to be food restricted until test day. On test day, mice

underwent Pavlovian approach testing, to assess cue-evoked sucrose seeking which consisted of a single session that was similar to the conditioning session, but under extinction conditions (i.e. in the absence of sucrose delivery in order to avoid the interference of acute sucrose consumption).

Fos immunohistochemistry

Following testing for Pavlovian approach, mice from the devaluation experiments remained in the conditioning chambers for an additional ~1 h to allow for optimal Fos expression. Subsequently, they were anaesthetized using sodium pentobarbital in saline (1:10, 200 mg/kg, i.p.). Mice were transcardially perfused with ice-cold PBS (concentrations in mM: NaCl 137, KCl 2.7, Na_2HPO_4 10, KH_2PO_4 1.8, pH 7.4) for 5 minutes (5 ml/min) and with ice-cold 4 % paraformaldehyde (PFA, Sigma-Aldrich cat. no. 158127) for 20 minutes (5 ml/min) using a peristaltic pump (Masterflex L/S, Cole Parmer). Thirty minutes after the end of the perfusion brains were removed, post-fixated in 4% PFA at 4 ºC for approximately 22 h, and then cryoprotected in 30% sucrose solution in PBS for 3-5 days. Brains were frozen on dry ice and stored at -80 ºC until further use. Brains were sliced into 30 µm coronal sections containing NAc (AP 1.5 from bregma; Paxinos, G and Franklin, 2012) using a cryostat (Leica CM 1900, Leica Microsystems) and stored in PBS with sodium azide (0.02%) or cryopreservant.

Free-floating slices were washed 3 times for 10 minutes in PBS, incubated in 0.3% hydrogen peroxide in PBS for 15-20 minutes to block endogenous peroxidase activity and subsequently washed 3 times in PBS. To block non-specific binding sites and permeabilize cell membranes, slices were incubated in 3% NGST (normal goat serum with Triton X-100; Vector Laboratories) for 1 h. Slices were incubated in primary antibody (rabbit anti c-Fos, sc-52, LOT: A2914, Santa Cruz Biotechnology, 1:8000, RRID:AB_2106783) in 3% NGST over night at 4 ºC. Next, slices were washed 3 times in PBS and incubated in the secondary

antibody (biotinylated goat anti-rabbit IgG H+L, Vector labs, 1:600, RRID:AB_2313606) in 1% NGST for 2 h. After 3 subsequent washes in PBS slices were incubated in ABC solution (RRID:AB_2336818, Vectorlabs) for 1 h and then washed twice in PBS. Slices were incubated in 0.04% DAB, 0.05% nickel ammonium sulfate, 0.04% hydrogen peroxide in PBS for approximately 30 minutes and washed 3 times in PBS. Slices were mounted in water onto Superfrost slides (Fisher) and dried overnight. For dehydration, slides went through the following steps: 2 x distilled water on ice 3 minutes, 30% ethanol 2 minutes, 60% ethanol 2 minutes, 90% ethanol 2 minutes, 95% ethanol 2 minutes, 100% ethanol 2 minutes, 100% ethanol 2 minutes, 2 x HistoClear (National Diagnostics) 10 minutes. Finally, slides were coversliped using Histomount (National Diagnostics), dried overnight and stored at room temperature.

Brightfield images of the NAc shell (hereafter NAc) were taken using a QI click camera (Qimaging) attached to an Olympus BX53 brightfield microscope and iVision-Mac software (Biovision Technologies, version 4.0.15, RRID: SCR_014786). Fos-positive neurons were counted manually bilaterally in a blind manner at a magnification of 100x using iVision software. Two images were taken per hemisphere (dorsal and ventral) and numbers of Fos-positive neurons were added to get one value per hemisphere. Between hemispheres values were averaged to get one value per animal. Our Fos analysis was restricted to medial proportions of the NAc due to low Fos expression in the lateral NAc.

Electrophysiology

Ex vivo *brain slice preparation*

Ninety minutes after the start of Pavlovian approach testing, mice were deeply anaesthetized with ketamine and xylazine (Anaesktin©, Dechra Veterinary Products; Rompun©, Bayer Healthcare) in saline, and then transcardially perfused with ice-cold NMDG solution (concentrations in mM: NMDG 93, KCl 2.5, NaH_2PO_4 1.2, $NaHCO_3$ 30, HEPES 20, D-

glucose 25, $C_6H_7NaO_6$ 5, $SC(NH_2)_2$ 2, $C_3H_3NaO_3$ 3, $MgSO_4H_20$ 10, $CaCl_2.2H_20$ 0.5, osmolarity 300 - 310 mOsm, pH 7.4) (Ting et al., 2018). Following perfusions, the brains were immersed in ice-cold filtered NMDG solution for 2 minutes. The cerebellum was removed and the brain was mounted onto a stage and placed in a slicing chamber filled with ice-cold NMDG solution. 250 µm thick coronal slices were cut corresponding to approximately 1.5 mm AP from Bregma. Slices were stored in NMDG solution for 5 minutes at 32 °C and then transferred to aCSF at room temperature until recording. NMDG solution and aCSF (artificial CSF, concentrations in mM: NaCl 126, KCl 4.5, $MgCl_2$ 1, $CaCl_2$ 2.5, NaH_2PO_4 1.2, D-glucose 11, $NaHCO_3$ 26, pH 7.4) were continuously bubbled with a 95% O_2:5% CO_2 mixture.

Electrophysiological recording

We recorded from NAc shell medium spiny neurons (MSNs) which are the principal neurons of this area using similar criteria as reported in (Ziminski et al., 2017). For NAc current clamp recordings, the slices were hemisectioned and transferred to the recording chamber continuously refilled with aCSF at 32 °C (flow rate approximately 2 ml/min). GFP+ neurons were identified using a 488 nm laser line from a Revolution XD spinning disk confocal system (Andor) attached to an Olympus BX51W1 microscope (Figure 3B). Whole-cell patch clamp recordings were performed using ICS (intracellular solution, concentrations in mM: K-gluconate 125, KCl 10, HEPES 10, $MgCl_2*6H_2O$ 2, EGTA 1, $CaCl_2*2H_2O_2$ 0.1, Mg-ATP 2, Na-GTP 0.2, pH 7.25)-filled borosilicate capillary glass-pipettes (inner diameter 0.86 mm, outer diameter 1.5 mm, resistance 5-7 MOhm; Sutter Instruments) using a P-97 electrode puller (Sutter Instruments). Alexa Fluor 568 dye (100 µM, cat. no. A10437, Thermo Fisher Scientific) was added to the ICS to confirm patched neurons by colocalization with GFP. MSNs were identified using morphology, resting membrane potential (RMP), and action potential (AP) waveform and held at -75 mV for the duration of the recordings. Liquid

junction potential was -13.7 mV and was not adjusted for. The current clamp recording protocol consisted of 800 ms current injections starting at -60 pA and increasing in 4 pA steps.

Data were collected with a Multiclamp 700B amplifier (Molecular Devices), WinEDR (version 3.7.5) and WinWCP Software (version 5.2.2, courtesy of Dr. John Dempster, University of Strathclyde, Glasgow, UK; http://spider.science.strath.ac.uk/sipbs/software_ses.htm, RRID: SCR_014713). Signals were digitized at 10 kHz and filtered at 5 kHz (PCI 6024E; National Instruments) and low-frequency noise was filtered out using a HumBug (Quest Scientific) module. The input resistance *(Ri)* was calculated as the slope of the I/V curve between -60 pA and 20 pA injections. Rheobase was calculated manually. Spike kinetics (amplitude and half-width) and afterhyperpolarization (AHP) were calculated using Mini Analysis Software (version 6.0; Synaptosoft, RRID:SCR_002184) and spike counts were calculated using Stimfit 0.14 software (Python 2.7.9) (Guzman et al., 2014). The amount of GFP+ and GFP– *neurons recorded per mouse* was kept approximately constant at 2-4 neurons in voltage clamp recordings and 4-6 neurons in current clamp and the order of recordings was counterbalanced.

Voltage clamp recordings were conducted in the presence of the $GABA_A$ receptor channel blocker, picrotoxin (100 µM; Sigma-Aldrich) using ICS (concentrations in mM: Spermine 0.1, $CsCH_3SO3$ 120, NaCl 5, TEA-Cl 10, HEPES 10, EGTA 1.1, MgATP 4, Na-GTP 0.3, QX314 4.6 (Lidocaine, Sigma-Aldrich). Spontaneous EPSCs (sEPSCs) were analyzed over a 30 s period. Responses were evoked through bipolar stimulating electrodes (FHC, CBASD75), within 400 µm of the neuron with 0.1 ms pulses at 0.033 Hz. Series resistance was monitored using -10 mV voltage steps (100 ms) and only neurons maintaining stable access (<15% change) were included in the analyses. Paired-pulse ratios (PPR) were calculated by stimulating twice in succession and dividing second peak by the first peak (average of

303 triplicate), across interstimulus intervals (ITIs) of 20, 40, 60, 80, 100, 150 and 200
304 milliseconds. AMPAR/NMDAR current ratios were calculated from the averages of 10-20
305 evoked EPSCs at +40 mV with and without D-APV (NMDA receptor antagonist, 50 μM, Hello
306 Bio). For each neuron, the AMPAR current (with D-APV) was subtracted from the combined
307 current (without D-APV) to yield the NMDAR current (Koya et al., 2012). AMPAR current
308 peak was divided by NMDAR current peak to yield AMPAR/NMDAR current ratios. AMPAR
309 rectification curves were produced by averaging triplicate stimulations at -80, -60, -40, -20, 0,
310 20 and 40 mV in the presence of D-APV. The AMPAR rectification index was calculated by
311 dividing the excitatory post-synaptic current (EPSC) peak amplitude at -80 mV by the peak
312 amplitude at +40 mV. The ratio of the chord conductance (G=I/V) was calculated by dividing
313 the chord conductance at +40 mV by the chord conductance at -80 mV ($G_{+40\ mV}$ / $G_{-80\ mV}$).
314 Traces in figures have stimulus artefacts removed.

315

316 Experimental Design and Statistical Analysis

317 Data were analyzed and visualized using GraphPad Prism 6 (Graphpad software,
318 RRID:SCR_002798), SPSS (IBM SPSS statistics, RRID:SCR_002865), and Excel
319 (Microsoft). Spontaneous EPSCs were analyzed using Mini Analysis Software (version 6.0;
320 Synaptosoft, RRID:SCR_002184) whereas evoked EPSCs (e.g. PPRs) were analyzed using
321 WinWCP Software. Statistical analyses are summarized in Table 2. All data are presented
322 as mean ± SEM. Data points exceeding ± 2 SD or greater from the mean were excluded
323 from the analyses. Group data are presented as mean ± SEM. ANOVAs were followed up by
324 Fisher's LSD test.

325

326 *Behavioral data*

Total number of head entries into the sucrose-delivery magazine during acquisition were analyzed using a two-way repeated measures ANOVA including cue presentation (ITI, CS) and session (1-12) as within-subjects factors. Two-way mixed ANOVAs were used to test for pre-existing differences in Pavlovian approach, using session (1-12) as within-subjects factor and caloric satiation (control, *ad lib* chow) or devaluation (Non-devalued, Devalued) as between-subjects factor. The test data was analyzed using two-way mixed ANOVAs using cue presentation (ITI, CS) as within-subjects factor and devaluation (Non-devalued, Devalued) or caloric satiation (Control, *ad lib* chow) as between-subjects factor. Body weights were analyzed using unpaired two-tailed t-tests. A total of four mice from the *ad lib* chow and Devalued groups were excluded from the test analyses due to equipment malfunction.

Fos expression

Fos quantification data was analyzed using a two-tailed t-test comparing the number of Fos+ neurons per square mm between Non-devalued and Devalued conditions. Brain sections from two mice were damaged and could not be used for cell quantification.

Electrophysiology

Spike counts and I/V curves were first analyzed using a three-way mixed ANOVA with devaluation (Non-devalued, Devalued) and GFP (+/–) as between-subjects factors and current step as the within-subjects factor. This was followed up by two-way mixed ANOVAs using current step as within-subjects factor and GFP (+/–) or devaluation (Non-devalued, Devalued) as between-subjects factor.

RMP, rheobase, Ri, AHP, spike amplitude and half-width were analyzed using two-way ANOVAs with devaluation (Non-devalued, Devalued) and GFP (+/–) as between-subject factors.

sEPSC frequency and amplitude, and AMPAR rectification index were analyzed using two-way ANOVAs with devaluation (Non-devalued, Devalued) and GFP (+/–) as between-subjects factors. The ratio of the chord conductance (G=I/V) at +40 mV over -80 mV ($G_{+40\ mV}$ / $G_{-80\ mV}$) was analyzed using a one-sample t-test against the population mean of 1, which indicates a lack of rectification (Bonferroni corrections were used to control for multiple comparisons). PPRs were analyzed using a three-way mixed ANOVA with devaluation (Non-devalued, Devalued) and GFP (+/–) as between-subjects factors and interstimulus interval as within-subjects factor. AMPAR/NMDAR current ratios and sEPSC parameters were analyzed using a two-way ANOVA with devaluation (Non-devalued, Devalued) and GFP (+/–) as between-subjects factors.

Results

Acquisition of Pavlovian conditioning

We assessed the establishment of a cue-sucrose association following 12 sessions of Pavlovian conditioning, during which an auditory cue (clicker) was repeatedly paired with 10% sucrose solution delivery (Figure 1A). With conditioning, mice made a significantly greater number of head entries into the sucrose delivery magazine during the CS period (cue and sucrose presentation) versus non-CS/ITI period; this difference was mainly due to a progressive decrease in responding during the ITI as conditioning progressed (Figure 1B). A two-way repeated measures ANOVA revealed a significant interaction of cue presentation (CS, ITI) and session ($F_{11,341}$ = 18.12, $p < 0.0001$) and significant main effects of cue presentation ($F_{1,31}$ = 321, $p < 0.0001$) and session ($F_{11,341}$ = 9.957, $p < 0.0001$). This finding indicates that mice learned the association between the cue and sucrose delivery.

Reward-specific devaluation attenuates Pavlovian approach

Seven days after the last acquisition session and after 4-6 days of either *ad lib* chow or sucrose solution in the home cage, mice underwent Pavlovian approach testing under extinction conditions (Figure 1A).

We first assessed the effect of sucrose devaluation on Pavlovian approach. A two-way mixed ANOVA showed a significant interaction of cue presentation x devaluation ($F_{1,28}$ = 5.275, $p = 0.0293$) and a significant effect of cue presentation ($F_{1,28}$ = 27.84, $p < 0.0001$). Post-hoc group differences are presented in Figure 1C, indicating a reduction of cue-evoked sucrose seeking in Devalued mice. Importantly, no pre-existing differences between groups were detected during acquisition (interaction of devaluation x session $F_{11, 330}$ = 0.6798, $p = 0.7577$; session $F_{11, 330}$ = 26.67, $p < 0.0001$; devaluation $F_{1, 30}$ = 0.016, $p = 0.9002$).

Frequent sucrose consumption results in weight gain (Te Morenga et al., 2013). Thus, as a measure for sucrose consumption, we measured the body weights of Devalued mice following *ad lib* sucrose consumption and compared them to Non-devalued mice. A t-test (t_{30} = 8.629, $p < 0.0001$) revealed that mice in the Devalued group exhibited significantly higher body weights than their Non-devalued counterparts (Figure 1D), indicating that mice in the Devalued group consumed a significant amount of sucrose.

Caloric satiation does not modulate Pavlovian approach

Next, we assessed whether increased caloric consumption alone would result in reduced cue reactivity. To this end we trained an additional group of mice using the same behavioral procedure as above, but instead of sucrose we provided them with *ad lib* chow in their home cage. Caloric satiation did not modulate cue-evoked sucrose seeking (Figure 1E), but cue presentations increased the number of head entries during the CS, as shown by a two-way ANOVA (interaction cue presentation x caloric satiation $F_{1,24}$ = 0.3335, p = 0.569, cue presentation $F_{1,24}$ = 14.26, p = 0.0009; caloric satiation $F_{1,24}$ = 1.081, p = 0.3089). Post-hoc comparisons are shown in Figure 1E. Again, no pre-existing differences between groups were detected during acquisition (interaction caloric satiation x session $F_{11, 308}$ = 0.8548, p = 0.5853; session $F_{11, 308}$ = 10.54, $p < 0.0001$; caloric satiation $F_{1, 28}$ = 0.907, p = 0.3491). Also, similar to *ad lib* sucrose consumption, *ad lib* chow also increased body weight (t_{26} = 10.62, $p < 0.001$; Figure 1F). This suggests that cue-evoked sucrose seeking was not attenuated by caloric need alone.

Devaluation attenuates NAc Fos expression

Next, we assessed the effects of reward-specific devaluation on neuronal ensemble activity in the NAc, by examining the number of Fos-expressing neurons (Figure 2A). A t-test

414 revealed a significant reduction in Fos positive neurons in NAc (t_{27} = 2.376, p = 0.0249) in
415 the Devalued group compared to Non-devalued group, indicating that a smaller ensemble
416 was recruited in the NAc following reward-specific devaluation (Figure 2B, C).

417

418 Devaluation is associated with lack of excitability differences between ensemble and non-
419 ensemble neurons.

420 In a separate cohort of mice, we assessed the excitability of cue-responsive, GFP+
421 'ensemble' and surrounding GFP– 'non-ensemble' MSNs 90 min following the initiation of
422 Pavlovian approach testing (Figure 3A). We injected increasing amounts of current into the
423 neurons and quantified the number of action potentials fired in response to assess the firing
424 capacity of these neurons (Figure 3). A three-way mixed ANOVA showed an interaction of
425 current step x devaluation x GFP ($F_{8, 304}$ = 3.115, p = 0.002), an interaction of current step x
426 GFP ($F_{8,304}$ = 6.784, p < 0.0001), as well as a significant main effect of current step ($F_{8,304}$ =
427 53.88, p < 0.0001) and GFP ($F_{1, 38}$ = 8.364, p = 0.006) but not devaluation ($F_{1, 38}$ = 0.012, p =
428 0.912). In order to determine what is driving this three-way interaction, we further conducted
429 a two-way ANOVA comparing the firing rates (spike counts) of GFP+ and GFP– neurons
430 within Non-devalued mice separately. This revealed an interaction of current step x GFP
431 ($F_{8,152}$ = 11.84, p < 0.0001), as well main effects of current step ($F_{8,152}$ = 35.64, p < 0.0001)
432 and GFP ($F_{1,19}$ = 18.57, p = 0.0004) (Figure 3C). This indicates that in Non-devalued mice,
433 GFP+ and GFP– neurons differed significantly in firing capacity. A similar ANOVA comparing
434 GFP+ and GFP– neurons within the Devalued group yielded a main effect of current step
435 ($F_{8,152}$ = 21.43, p < 0.0001), but no effect of GFP ($F_{1, 19}$ = 0.3584, p = 0.5565) or interaction
436 ($F_{8, 152}$ = 0.5413, p = 0.8239) (Figure 3D). Hence, in the Devalued group GFP+ and GFP–
437 neurons did not differ in firing capacity. Post-hoc tests are indicated in Figure 3C, D). Taken
438 together, these results indicate that differences in excitability between GFP+ and GFP–
439 neurons are eliminated following reward-specific devaluation.

Excitability changes in both ensemble and non-ensemble neurons underlie alterations in appetitive learning (Whitaker et al., 2017; Ziminski et al., 2017, 2018). Therefore, we compared the spike counts of GFP+ and GFP– neurons separately across conditions. For the GFP– non-ensemble neurons (Figure 3E), we discovered an interaction of current step x devaluation ($F_{8,152}$ = 2.048, p = 0.0444), a main effect of current step ($F_{8,152}$ = 15.91, p < 0.0001) but no main effect of devaluation ($F_{1, 19}$ = 3.271, p = 0.0864). Post-hoc analysis revealed a slight, but significant increase in spike number in GFP– neurons from the Devalued group, which was not accompanied by any changes in the I/V curves nor any of the active and passive membrane properties (Figure 3, 4). For the GFP+ ensemble (Figure 3F), two-way mixed ANOVAs revealed no significant interaction of current step x devaluation ($F_{8, 152}$ = 1.33, p = 0.2324) or main effect of devaluation ($F_{1, 19}$ = 1.152, p = 0.2966) but a significant main effect of current step ($F_{8,152}$ = 38.45, p < 0.0001). These findings indicate that a slight increase in excitability in GFP– non-ensemble neurons contributed to the lack of excitability differences between the GFP+ and GFP– neurons as a function of reward-specific devaluation.

Analysis of I/V curves with a three-way mixed ANOVA did not reveal aninteraction of current step x GFP x devaluation ($F_{20, 780}$ = 1.212, p = 0.236) but a significant interaction of current step x GFP ($F_{20, 780}$ = 11.031, p < 0.0001), as well as a significant effect of current step ($F_{20, 780}$ = 430.768, p < 0.0001), GFP ($F_{1,39}$ = 16.829, p < 0.0001), but not devaluation ($F_{1, 39}$ = 0.789, p = 0.38). To determine what is driving these effects, further analysis using a two-way ANOVA comparing GFP+ and GFP– neurons separately within Non-devalued and Devalued groups was conducted. It revealed a significant interaction of current step x GFP ($F_{20,360}$ = 7.951, p < 0.0001), as well as main effects of each factor (current step $F_{20,360}$ = 185.5, p < 0.0001; GFP $F_{1,18}$ = 11.5, p = 0.0033) in the Non-devalued group (Figure 3C inlay), similar to the effect observed in the number of spikes. Post-hoc comparisons between GFP+ and GFP– neurons in negative and positive potential are indicated in Figure 3C inlay. In the Devalued group, a two-way ANOVA comparing GFP+ and GFP– neurons yielded an

interaction of current step x GFP ($F_{20,380}$ = 2.931, p < 0.0001), as well as main effect of both factors (current step $F_{20,380}$ = 217.6, p < 0.0001, GFP $F_{1,19}$ = 4.504, p = 0.0472, Figure 3D inlay). Post-hoc tests are indicated in Figure 3D inlay. Similar to our previous analysis of excitability, we next conducted additional two-way ANOVAs in GFP+ or GFP– neurons between the Devalued and Non-devalued groups. For both, GFP+ and GFP– neurons, no significant interaction or effect of GFP, but an effect of current step (GFP+: $F_{20, 360}$ = 177.5, p < 0.0001, GFP–: $F_{20,380}$ = 267.7, p < 0.0001) were revealed (Figure 3 E, F inlays). In summary, the differences in the I/V curves of GFP + and GFP– neurons seen prior to devaluation were still present afterwards, but less pronounced and restricted to negative potentials.

To investigate the source of the differences in firing capacity, we examined the resting membrane potential (RMP), rheobase, Ri, AHP, and AP half-width and amplitude of GFP+ and GFP– neurons from Non-Devalued and Devalued groups using two-way ANOVAs (Figure 4, Table 1). For rheobase ($F_{1,37}$ = 4.57, p = 0.0392, Figure 4B), but none of the remaining parameters, we found a significant interaction of devaluation x GFP. Post-hoc testing revealed decreased rheobase in GFP+ neurons compared to GFP– neurons in the Non-Devalued, but not Devalued group. This suggests that devaluation eliminated the differences in the minimum amount of current needed for spiking between ensemble and non-ensemble neurons (Table 1). We only found a main effect of GFP for Ri, ($F_{1,38}$ = 13.47, p = 0.0007, Figure 4C) and AP half-width ($F_{1,37}$ = 6.004, p = 0.012, Figure 4D). There was a main effect for devaluation for AHP ($F_{1,38}$ = 6.07, p = 0.02, Figure 4E), AP half-width ($F_{1,37}$ = 4.31, p = 0.04, Figure 4D) and rheobase ($F_{1,37}$ = 7.02, p = 0.01, Figure 4B). Post-hoc tests are indicated in Figure 4 and Table 1. We did not reveal any effects on RMP and AP amplitude (Figure 4 A, F). Hence, devaluation did not modulate these properties in an ensemble-specific manner.

493 Devaluation does not modulate synaptic properties in an ensemble-specific manner

494 We next investigated the synaptic properties of GFP+ and GFP– neurons in Non-devalued
495 and Devalued groups. We first measured the synaptic strength in these neurons by
496 assessing the AMPAR/NMDAR ratios. A two-way ANOVA did not reveal a significant
497 interaction of devaluation x GFP ($F_{1, 19}$ = 0.35, p = 0.56, Figure 5A), indicating a lack of
498 differences in synaptic strength across ensembles and conditions. The insertion of GluA2-
499 lacking AMPARs enhances excitatory transmission and neurons expressing these receptors
500 display inward rectification (Cull-Candy et al., 2006). Therefore, we measured rectification of
501 AMPAR EPSC by dividing the EPSC amplitude at -80 mV by the amplitude at +40 mV in the
502 presence of the NMDA-antagonist APV. We observed no significant interaction of GFP x
503 devaluation ($F_{1, 15}$ = 0.37, p = 0.55, Figure 5B), indicating no differences in the expression of
504 GluA2-lacking AMPARs across ensembles and conditions.

505 Previous studies have shown that food restriction and palatable food consumption increase
506 the expression of GluA2-lacking AMPARs in the nucleus accumbens (Oginsky et al., 2016;
507 Ouyang et al., 2017). As such, we examined whether inward rectification was generally
508 present in Devalued and Non-devalued mice that underwent both food restriction and
509 repeated sucrose consumption during training. We calculated the ratio of the chord
510 conductance (G) at +40 mV over -80 mV ($G_{+40\ mV}$ / $G_{-80\ mV}$). If rectification is present, then this
511 value is lower than 1. A one-sample t-test against a population of mean of 1 revealed that in
512 the Devalued group, GFP+ neurons did not display rectification (0.70 ± 0.11; t_4 = 2.67, p =
513 0.0559), but was observed in GFP– neurons (0.58 ± 0.09; t_4 = 4.48, p = 0.0110). Also,
514 rectification was observed in GFP+ and GFP– neurons in the Non-devalued group (GFP+:
515 0.57 ± 0.02, t_3 = 20.16, p = 0.0003; GFP–: 0.56 ± 0.04, t_4 = 10.32, p = 0.0005). Collectively,
516 these data suggest that devaluation did not modulate synaptic strength and AMPA receptor
517 function on NAc ensembles. However, these data suggest that we observed widespread
518 expression of GluA2-lacking AMPARs, as indicated by rectification in GFP– non-ensemble
519 neurons regardless of Devaluation.

Next, we examined the sEPSC frequency and amplitude. We observed no significant interaction of GFP x devaluation in sEPSC frequency ($F_{1, 65}$ = 0.03, p = 0.85, Figure 5C) or amplitude ($F_{1,65}$ = 0.71, p = 0.40, Figure 5C). There was a main effect of devaluation for sEPSC frequency ($F_{1, 65}$ = 6.46, $p<0.05$), suggesting a generalized decrease in sEPSC frequency in Devalued mice (Figure 5C). Finally, we observed no interaction or main effects in presynaptic release probability as measured using the PPR (GFP x devaluation x interstimulus interval $F_{6,180}$ = 0.53, p = 0.78), suggesting the group differences in sEPSC frequency were not driven by presynaptic adaptations (Figure 5D).

Discussion

Here we examined the effects of devaluation on ensemble plasticity at the levels of recruitment, excitability, and synaptic physiology in sucrose conditioned *Fos-GFP* mice. After conditioning we provided mice with four days of *ad lib* sucrose or standard chow. Sucrose access, but not caloric satiation alone attenuated cue-evoked sucrose seeking and hence led to devaluation. This reward-specific devaluation: i) reduced the size of the behaviorally-activated NAc shell neuronal ensemble; ii) eliminated differences in excitability between ensemble and non-ensemble neurons that was observed under Non-devalued conditions. Interestingly, devaluation did not alter any ensemble-specific synaptic alterations. Our findings provide new insights into how changes in the rewarding properties of food modulate cue-evoked sucrose seeking by potentially modifying the background excitability of NAc non-ensemble neurons.

Implications and mechanisms of reduced cue-evoked sucrose seeking and ensemble size following devaluation

Reward-specific devaluation, but not general caloric satiation alone, decreased cue-evoked sucrose seeking. Hence, the incentive and/or hedonic properties of sucrose, but not homeostatic need may control this behavioral change. The incentive properties relate to the inclination to seek food, whereas the hedonic properties relate to the pleasurable properties associated with food consumption (Castro et al., 2015). One possibility then is that *ad lib* sucrose decreased the sucrose-associated cue's incentive properties. In support, selective satiation reduces breakpoints on a progressive-ratio appetitive task (Baxter et al., 2000). Alternatively, mice in our study may have updated the reward representation according to the new and less attractive value and adapted their food-seeking because sucrose overconsumption lead to decreases in palatability or hedonic properties (Thompson et al. 1976; Strickland at al., 2018). In order to directly determine the factors that decreased

555 sucrose seeking, a future study incorporating sucrose consumption and orofacial reactivity
556 during a sucrose consumption test would be needed (Berridge et al., 1981; Castro et al.,
557 2015; Johnson et al., 2009).

558 Devaluation decreased NAc Fos expression consistent with NAc's role in mediating the
559 hedonic and incentive properties of sucrose and associated cues (Kelley et al., 1996; Taha,
560 2005; Cacciapaglia et al., 2012). At the circuit level, neuronal activation after devaluation
561 may be reduced via inhibition from local interneurons that control ensemble size.
562 Additionally, decreased excitatory drive from cortical afferents mediating goal-directed
563 behaviors from areas such as the basolateral amygdala and ventral hippocampus may
564 contribute (Taverna et al., 2005; Wilson, 2007; Shiflett & Balleine, 2010; Stefanelli et al.,
565 2016; LeGates et al., 2018). The result is reduced output into areas such as the lateral
566 hypothalamus and ventral tegmental area, and thus attenuation of cue-evoked sucrose
567 seeking (Kelley et al., 2005; Castro et al., 2015; Yang et al., 2018).

568 NAc neurons expressing either the dopamine 1 or 2 receptor (D1R, D2R) project to different
569 mesocorticolimbic structures and play distinct roles in reward-related behaviors (Smith et al.,
570 2013). Here, we did not distinguish neurons based on their D1R/D2R expression. It has
571 recently been observed that conditioning and extinction learning does not modulate the
572 proportion of D1R- and D2R-expressing ensembles following cue exposure (Ziminski et al.,
573 2017). Also, there are no clear differences in goal-directed behavior upon optogenetic
574 stimulation of either subpopulation (Natsubori et al., 2017). Hence, it is likely that devaluation
575 recruits an ensemble with similar levels of D1R and D2R-expressing neurons. However,
576 additional investigations are necessary to confirm this.

577

578 Implications for lack of ensemble excitability differences following devaluation

579 Following reward-specific devaluation, the previous excitability differences observed
580 between ensemble and non-ensemble neurons were eliminated. *In vivo*, such shifts in

581 excitability may modulate neuronal firing in response to cue presentations. In support,
582 devaluation reduces the number of phasically firing NAc neurons in response to sucrose
583 cues (West & Carelli, 2016). But what is the identity of this ensemble activated following
584 devaluation that does not differ in excitability from non-ensemble neurons? After devaluation
585 we may have recorded from a smaller subset of the *same* ensemble that was activated
586 under Non-devalued conditions during sucrose seeking, which may have updated the cue-
587 reward association. Alternatively, others have reported that ensembles that promote and
588 inhibit food-seeking co-exist in the same brain area (Suto et al., 2016; Warren et al., 2016).
589 Therefore, after devaluation we may have recorded from a *different* and incidentally smaller
590 ensemble which represented the changed reward value. While distinguishing these two
591 possibilities is challenging, future studies may longitudinally monitor cue-activated NAc
592 neurons with and without devaluation and functionally interrogate them using
593 opto/chemogenetics to determine which of the above possibilities are relevant.

594 The elimination of excitability differences between ensemble and non-ensemble neurons
595 following devaluation arose from a slight enhancement of excitability only in non-ensemble
596 neurons. These excitability differences are thought to boost the signal-to-noise ratio of
597 information processing of ensemble neurons (Nicola et al., 2000; Ziminski et al., 2018) and
598 its elimination may thus attenuate the responsivity to food-associated cues following
599 devaluation. The cause for this increased background excitability is unclear, but we note that
600 sucrose consumption increases NAc shell dopamine transmission (Roitman et al., 2008).
601 This dopamine release resulting from daily sucrose consumption may enhance MSN
602 excitability through D1R activation (Hernandez-Lopez et al., 1997). Here, we did not observe
603 any associated changes in active and passive membrane properties in these non-ensemble
604 neurons. This observed lack of change may have resulted from not distinguishing our NAc
605 MSNs based on dopamine receptor-expression, which may have masked any subtle cell-
606 type specific changes. Finally, enhancements in firing capacity have been observed
607 following D1R activation without any changes in Ri, spike threshold, and duration (Tseng &

608 O'Donnell, 2004), despite the known role of D1R activation enhancing L-type Ca^{+2} currents
609 that regulate repetitive firing (Hernandez-Lopez et al., 1997). This indicates that subtle
610 changes in passive and active membrane properties may not always be detected despite
611 alterations in firing capacity. Further studies are required to parse out the cellular and
612 intrinsic factors that resulted in this minor, but widespread enhancement in neuronal firing
613 following devaluation.

614

615 Potential reasons for lack of learning- or devaluation-induced ensemble specific differences
616 in synaptic physiology

617 Surprisingly, despite the role of glutamate synapse alterations in appetitive learning, we
618 found no alterations in sEPSC frequency and amplitude, AMPAR/NMDAR current ratio,
619 AMPA rectification index, and PPR. We however observed a generalized reduction in
620 sEPSC frequency, indicating synaptic alterations induced by *ad lib* sucrose consumption.
621 This contrasts with studies using drug rewards demonstrating increased spine dynamics in
622 NAc ensembles selectively activated in response to drug-associated cues (Singer et al.,
623 2016; Whitaker et al., 2016). This difference between natural and drug rewards in their ability
624 to generate synaptic alterations in NAc may be due to natural rewards being less potent at
625 eliciting behavioral and neurophysiological changes (Grimm et al., 2003; Chen et al., 2008;
626 Gipson et al., 2013). Additionally, for associative learning paradigms using natural
627 reinforcers, an extended timeframe, or paradigms with more CS-US pairings may be needed
628 to induce synaptic alterations (Cifani et al., 2012; Guegan et al., 2013a; Counotte et al.,
629 2014). Taken together, the lack of indices of plasticity at glutamatergic synapses we
630 demonstrate in NAc neuronal ensembles may reflect inherent differences of natural and drug
631 rewards and the way their behavioral outcomes are manifested.

632

633 The role of ensemble changes in intrinsic excitability, but not synaptic physiology

Few studies to date have examined the role of both intrinsic and synaptic plasticity in appetitive associative learning. So far, fear conditioning studies have demonstrated the concomitant alterations of intrinsic excitability and synaptic physiology following associative learning (Rosenkranz & Grace, 2002). In contrast, we found neuronal excitability, but not excitatory synaptic physiology to be altered by devaluation. In line with our findings, previous studies have reported excitability changes independently of synaptic plasticity (Egorov et al., 2002; Labno et al., 2014). It is proposed that alterations in excitability may serve as a transient priming mechanism for initial associative memory formation before synaptic changes take place (Moyer et al., 1996; Janowitz & Van Rossum, 2006; Mozzachiodi & Byrne, 2010). Further research is needed to determine if our observed excitability changes constitute a transient priming mechanism active during rule learning of the updated reward value and whether synaptic alterations consolidating this updated value might be detectable later on.

Limitations and conclusion

Reward-specific devaluation, but not caloric satiation, attenuated cue-evoked sucrose seeking. Thus, it is conceivable that the associated physiological effects on Fos expression and ensemble excitability are due to a decreased value of sucrose reward. However, the present study cannot rule out the possibility that our observed Fos and excitability alterations were modulated by caloric satiety provided during sucrose devaluation. Therefore, even though caloric satiation alone did not attenuate sucrose seeking, it would be critical in future studies to determine whether caloric satiation attenuates Fos expression and eliminates excitability differences between ensemble and non-ensemble neurons in the absence of CS exposure.

Fos expression requires sustained neuronal activity and therefore only labels strongly activated neurons, which play a role in cue-evoked behaviours (Koya et al., 2009; Cruz et

al., 2013; Warren et al., 2016; Whitaker et al., 2016). In *Fos-GFP* rats and mice, GFP is co-expressed with Fos and peaks 2 hours after induction and is back to baseline by 24 hours (Barth, 2004; Cifani et al., 2012; Koya et al., 2012). Hence, it is unlikely that many of the GFP+ neurons in the current study were activated long before the Pavlovian approach test, although GFP+ neurons might have been activated by other events close in time. Thus, in our Devalued group, recent sucrose consumption may have induced Fos (Sheng & Greenberg, 1990; Cruz et al., 2015). However, Fos induction in the striatum habituates rapidly and consumption of a sweet solution has been shown to not alter Fos expression in NAc (Duncan et al., 1996; Struthers et al., 2005). Hence, our GFP+ neurons likely represent neurons activated during Pavlovian approach testing rather than recent sucrose consumption. However, to establish this possibility we would need to employ strategies that would label neurons activated by both recent sucrose consumption and CS exposure. Activity-sensitive immediate early genes, *homer1a* and *arc,* may be useful for such studies as they are used to label neurons activated by distinct stimuli presented at two different time points (Grosso et al., 2015).

Differences in Fos induction based on satiety state have been observed previously. *Ad lib* chow maintained rats exhibited no change in NAc Fos protein or mRNA upon consumption of a sweet solution or pellets (Duncan et al., 1996; Gao et al., 2017). However, when mice are food restricted, palatable food consumption has been shown to increase Fos expression in NAc (Latagliata et al., 2018). In the current study, we did not see this satiety-based increase in Fos, as after 4 days of sucrose consumption effects of reward devaluation on Fos expression may outweigh the satiety effects of sucrose consumption, resulting in the observed decrease in Fos levels. In order to shed light on this, future studies could investigate Fos levels after shorter periods of sucrose consumption.

In this study, all of our mice were trained under ‘Paired’ conditions in which CS and US presentations occurred in temporal proximity. We did not employ an ‘Unpaired’ control group

688 which receives CS and US presentations at disparate times (e.g. CS in the conditioning
689 chamber, US in the home cage) to prevent their association. This control group is used to
690 parse out neuronal activation and excitability patterns that are induced by general stimuli that
691 are not explicitly paired with the US. We observed enhanced excitability in CS-activated
692 neurons in our Non-Devalued control group. Ziminski and colleagues (2017) demonstrated in
693 *Fos-GFP* mice that sucrose-associated CS's increased GFP expression by 1.4-fold and
694 recruited a hyper-excitable GFP+ ensemble in Paired compared to the Unpaired group.
695 These additional GFP+ neurons likely represent those that are recruited by sucrose cue
696 exposure. Thus, the ensemble hyper-excitability in the Non-devalued control group occurred
697 as a result of the CS being paired with sucrose and is not a general property of activated
698 neurons. Interestingly, Fos expression decreased by 1.4-fold following devaluation (Figure
699 2B), which suggests that devaluation reduced Fos expression related to sucrose cue
700 exposure. However, it remains to be determined if *ad lib* sucrose consumption alone is
701 capable of attenuating Fos expression in Unpaired mice.
702
703 As Devalued mice made fewer head entries during the CS they may have experienced a
704 reduced amount of extinction learning compared to Non-devalued mice. These differences in
705 extinction learning may have elicited devaluation-independent consequences on NAc
706 activation patterns and hence decreased Fos expression. However, Ziminski and colleagues
707 demonstrated that extinction learning decreased NAc *Fos* expression (Ziminski et al., 2017).
708 As Non-devalued mice with more opportunity for extinction learning expressed more Fos
709 than Devalued mice, this reduction is unlikely due to the reduced opportunity to engage in
710 extinction learning in Devalued mice.
711
712 Here we revealed that devaluation was associated with altered ensemble size and intrinsic
713 excitability, but not synaptic plasticity in behaviourally activated neuronal ensembles in the
714 NAc shell. Our findings reveal novel mechanisms underlying cognitive and behavioural
715 flexibility. However, future studies are required to elucidate the functional role of devaluation-

activated neuronal ensembles. For instance, chemogenetic or optogenetic approaches using *Fos-tTA* mice that allow tagging and stimulation of Fos-expressing neurons will allow us to reveal if activation of Fos-expressing neurons following Devaluation is sufficient to reduce cue-evoked sucrose seeking (Cruz et al., 2013). Additionally, we need to identify the afferent brain areas that regulate these forms of ensemble plasticity and the downstream areas that are modulated as a result to further elucidate mechanisms that suppress food seeking. Such processes are important to understand why certain individuals are hypersensitive to food cues and resistant to internal signals that help limit food intake.

References

Barth, A. L. (2004). Alteration of Neuronal Firing Properties after In Vivo Experience in a FosGFP Transgenic Mouse. *Journal of Neuroscience*. https://doi.org/10.1523/JNEUROSCI.4737-03.2004

Baxter, M. G., Parker, A., Lindner, C. C., Izquierdo, A. D., & Murray, E. A. (2000). Control of response selection by reinforcer value requires interaction of amygdala and orbital prefrontal cortex. *The Journal of Neuroscience : The Official Journal of the Society for Neuroscience*, *20*(11), 4311–4319. Retrieved from http://www.ncbi.nlm.nih.gov/pubmed/10818166

Berridge, K., Grill, H. J., & Norgren, R. (1981). Relation of consummatory responses and preabsorptive insulin release to palatability and learned taste aversions. *Journal of Comparative and Physiological Psychology*, *95*(3), 363–382. https://doi.org/10.1037/h0077782

Boswell, R. G., & Kober, H. (2016). Food cue reactivity and craving predict eating and weight gain: A meta-analytic review. *Obesity Reviews*. https://doi.org/10.1111/obr.12354

Cacciapaglia, F., Saddoris, M. P., Wightman, R. M., & Carelli, R. M. (2012). Differential dopamine release dynamics in the nucleus accumbens core and shell track distinct aspects of goal-directed behavior for sucrose. *Neuropharmacology*. https://doi.org/10.1016/j.neuropharm.2011.12.027

Carelli, R. M., Ijames, S. G., & Crumling, a J. (2000). Evidence that separate neural circuits in the nucleus accumbens encode cocaine versus “natural” (water and food) reward. *The Journal of Neuroscience : The Official Journal of the Society for Neuroscience*. https://doi.org/20/11/4255 [pii]

Castro, D. C., Cole, S. L., & Berridge, K. C. (2015). Lateral hypothalamus, nucleus accumbens, and ventral pallidum roles in eating and hunger: interactions between

homeostatic and reward circuitry. *Frontiers in Systems Neuroscience*, *9*, 90. https://doi.org/10.3389/fnsys.2015.00090

Chen, B. T., Bowers, M. S., Martin, M., Hopf, F. W., Guillory, A. M., Carelli, R. M., … Bonci, A. (2008). Cocaine but Not Natural Reward Self-Administration nor Passive Cocaine Infusion Produces Persistent LTP in the VTA. *Neuron*. https://doi.org/10.1016/j.neuron.2008.05.024

Cifani, C., Koya, E., Navarre, B. M., Calu, D. J., Baumann, M. H., Marchant, N. J., … Hope, B. T. (2012). Medial Prefrontal Cortex Neuronal Activation and Synaptic Alterations after Stress-Induced Reinstatement of Palatable Food Seeking: A Study Using c-fos-GFP Transgenic Female Rats. *Journal of Neuroscience*. https://doi.org/10.1523/JNEUROSCI.5895-11.2012

Counotte, D. S., Schiefer, C., Shaham, Y., & O'Donnell, P. (2014). Time-dependent decreases in nucleus accumbens AMPA/NMDA ratio and incubation of sucrose craving in adolescent and adult rats. *Psychopharmacology*, *231*(8), 1675–1684. https://doi.org/10.1007/s00213-013-3294-3

Cruz, F. C., Javier Rubio, F., & Hope, B. T. (2015). Using c-fos to study neuronal ensembles in corticostriatal circuitry of addiction. *Brain Research*. https://doi.org/10.1016/j.brainres.2014.11.005

Cruz, F. C., Koya, E., Guez-Barber, D. H., Bossert, J. M., Lupica, C. R., Shaham, Y., & Hope, B. T. (2013). New technologies for examining the role of neuronal ensembles in drug addiction and fear. *Nature Reviews. Neuroscience*, *14*(11), 743–754. https://doi.org/10.1038/nrn3597

Cull-Candy, S., Kelly, L., & Farrant, M. (2006). Regulation of Ca2+-permeable AMPA receptors: synaptic plasticity and beyond. *Current Opinion in Neurobiology*. https://doi.org/10.1016/j.conb.2006.05.012

775 Day, J. J., & Carelli, R. M. (2007). The nucleus accumbens and pavlovian reward learning.
776 *Neuroscientist*. https://doi.org/10.1177/1073858406295854

777 Duncan, G. E., Knapp, D. J., & Breese, G. R. (1996). Neuroanatomical characterization of
778 Fos induction in rat behavioral models of anxiety. *Brain Research*.
779 https://doi.org/10.1016/0006-8993(95)01486-1

780 Egorov, A. V., Hamam, B. N., Fransén, E., Hasselmo, M. E., & Alonso, A. A. (2002). Graded
781 persistent activity in entorhinal cortex neurons. *Nature*.
782 https://doi.org/10.1038/nature01171

783 Gao, P., Limpens, J. H. W., Spijker, S., Vanderschuren, L. J. M. J., & Voorn, P. (2017).
784 Stable immediate early gene expression patterns in medial prefrontal cortex and
785 striatum after long-term cocaine self-administration. *Addiction Biology*.
786 https://doi.org/10.1111/adb.12330

787 Gipson, C. D., Kupchik, Y. M., Shen, H., Reissner, K. J., Thomas, C. A., & Kalivas, P. W.
788 (2013). Relapse induced by cues predicting cocaine depends on rapid, transient
789 synaptic potentiation. *Neuron*. https://doi.org/10.1016/j.neuron.2013.01.005

790 Goldstone, A. P., Prechtl de Hernandez, C. G., Beaver, J. D., Muhammed, K., Croese, C.,
791 Bell, G., … Bell, J. D. (2009). Fasting biases brain reward systems towards high-calorie
792 foods. *The European Journal of Neuroscience*, *30*(8), 1625–1635.
793 https://doi.org/10.1111/j.1460-9568.2009.06949.x

794 Grimm, J. W., Lu, L., Hayashi, T., Hope, B. T., Su, T.-P., & Shaham, Y. (2003). Time-
795 dependent increases in brain-derived neurotrophic factor protein levels within the
796 mesolimbic dopamine system after withdrawal from cocaine: implications for incubation
797 of cocaine craving. *The Journal of Neuroscience : The Official Journal of the Society for*
798 *Neuroscience*, *23*(3), 742–747.

799 Grosso, A., Cambiaghi, M., Renna, A., Milano, L., Roberto Merlo, G., Sacco, T., & Sacchetti,

800 B. (2015). The higher order auditory cortex is involved in the assignment of affective
801 value to sensory stimuli. *Nature Communications*. https://doi.org/10.1038/ncomms9886

802 Guegan, T., Cutando, L., Ayuso, E., Santini, E., Fisone, G., Bosch, F., … Martin, M. (2013).
803 Operant behavior to obtain palatable food modifies neuronal plasticity in the brain
804 reward circuit. *European Neuropsychopharmacology*.
805 https://doi.org/10.1016/j.euroneuro.2012.04.004

806 Guegan, T., Cutando, L., Gangarossa, G., Santini, E., Fisone, G., Martinez, A., … Martin, M.
807 (2013). Operant behavior to obtain palatable food modifies ERK activity in the brain
808 reward circuit. *European Neuropsychopharmacology*.
809 https://doi.org/10.1016/j.euroneuro.2012.04.009

810 Guzman, S. J., Schlögl, A., & Schmidt-Hieber, C. (2014). Stimfit: quantifying
811 electrophysiological data with Python. *Frontiers in Neuroinformatics*, *8*, 16.
812 https://doi.org/10.3389/fninf.2014.00016

813 Hernandez-Lopez, S., Bargas, J., Surmeier, D. J., Reyes, A., & Galarraga, E. (1997). D1
814 receptor activation enhances evoked discharge in neostriatal medium spiny neurons by
815 modulating an L-type Ca2+ conductance. *The Journal of Neuroscience : The Official*
816 *Journal of the Society for Neuroscience*, *17*(9), 3334–3342.

817 Holland, P. C., & Rescorla, R. A. (1975). The Effect of Two Ways of Devaluating the
818 Unconditioned Stimulus after First- and Second-Prder Appetitive Conditioning. *Journal*
819 *of Experimental Psychology: Animal Behavior Processes*, *1*(4), 355–363.

820 Janowitz, M. K., & Van Rossum, M. C. W. (2006). Excitability changes that complement
821 Hebbian learning. *Network: Computation in Neural Systems*.
822 https://doi.org/10.1080/09548980500286797

823 Jansen, A., Schyns, G., Bongers, P., & van den Akker, K. (2016). From lab to clinic:
824 Extinction of cued cravings to reduce overeating. *Physiology & Behavior*, *162*, 174–180.

https://doi.org/10.1016/j.physbeh.2016.03.018

Johnson, A. W., Gallagher, M., & Holland, P. C. (2009). The Basolateral Amygdala Is Critical to the Expression of Pavlovian and Instrumental Outcome-Specific Reinforcer Devaluation Effects. *Journal of Neuroscience*. https://doi.org/10.1523/JNEUROSCI.3758-08.2009

Jones, S., Sample, C. H., Hargrave, S. L., & Davidson, T. L. (2018). Associative mechanisms underlying the function of satiety cues in the control of energy intake and appetitive behavior. *Physiology & Behavior*, *192*, 37–49. https://doi.org/10.1016/j.physbeh.2018.03.017

Kelley, A E, Bless, E. P., & Swanson, C. J. (1996). Investigation of the effects of opiate antagonists infused into the nucleus accumbens on feeding and sucrose drinking in rats. *The Journal of Pharmacology and Experimental Therapeutics*, *278*(3), 1499–1507.

Kelley, Ann E., Baldo, B. A., & Pratt, W. E. (2005). A proposed hypothalamic-thalamic-striatal axis for the integration of energy balance, arousal, and food reward. *Journal of Comparative Neurology*. https://doi.org/10.1002/cne.20769

Kelley, Ann E. (2004). Ventral striatal control of appetitive motivation: role in ingestive behavior and reward-related learning. *Neuroscience and Biobehavioral Reviews*, *27*(8), 765–776. https://doi.org/10.1016/j.neubiorev.2003.11.015

Kosheleff, A. R., Araki, J., Tsan, L., Chen, G., Murphy, N. P., Maidment, N. T., & Ostlund, S. B. (2018). Junk food exposure disrupts selection of food-seeking actions in rats. *Frontiers in Psychiatry*. https://doi.org/10.3389/fpsyt.2018.00350

Kourrich, S., Calu, D. J., & Bonci, A. (2015). Intrinsic plasticity: An emerging player in addiction. *Nature Reviews Neuroscience*. https://doi.org/10.1038/nrn3877

Koya, E., Cruz, F. C., Ator, R., Golden, S. A., Hoffman, A. F., Lupica, C. R., & Hope, B. T.

(2012). Silent synapses in selectively activated nucleus accumbens neurons following cocaine sensitization. *Nature Neuroscience*. https://doi.org/10.1038/nn.3232

Koya, E., Golden, S. A., Harvey, B. K., Guez-Barber, D. H., Berkow, A., Simmons, D. E., … Hope, B. T. (2009). Targeted disruption of cocaine-activated nucleus accumbens neurons prevents context-specific sensitization. *Nature Neuroscience*, *12*(8), 1069–1073.

Labno, A., Warrier, A., Wang, S., & Zhang, X. (2014). Local plasticity of dendritic excitability can be autonomous of synaptic plasticity and regulated by activity-based phosphorylation of Kv4.2. *PLoS ONE*. https://doi.org/10.1371/journal.pone.0084086

Latagliata, E. C., Puglisi-Allegra, S., Ventura, R., & Cabib, S. (2018). Norepinephrine in the Medial Pre-frontal Cortex Supports Accumbens Shell Responses to a Novel Palatable Food in Food-Restricted Mice Only. *Frontiers in Behavioral Neuroscience*. https://doi.org/10.3389/fnbeh.2018.00007

LeGates, T. A., Kvarta, M. D., Tooley, J. R., Francis, T. C., Lobo, M. K., Creed, M. C., & Thompson, S. M. (2018). Reward behaviour is regulated by the strength of hippocampus–nucleus accumbens synapses. *Nature*. https://doi.org/10.1038/s41586-018-0740-8

Moyer, J. R., Thompson, L. T., & Disterhoft, J. F. (1996). Trace eyeblink conditioning increases CA1 excitability in a transient and learning-specific manner. *The Journal of Neuroscience : The Official Journal of the Society for Neuroscience*.

Mozzachiodi, R., & Byrne, J. H. (2010). More than synaptic plasticity: role of nonsynaptic plasticity in learning and memory. *Trends in Neurosciences*. https://doi.org/10.1016/j.tins.2009.10.001

Natsubori, A., Tsutsui-Kimura, I., Nishida, H., Bouchekioua, Y., Sekiya, H., Uchigashima, M., … Tanaka, K. F. (2017). Ventrolateral Striatal Medium Spiny Neurons Positively

874 Regulate Food-Incentive, Goal-Directed Behavior Independently of D1 and D2
875 Selectivity. *The Journal of Neuroscience*. https://doi.org/10.1523/JNEUROSCI.3377-
876 16.2017

877 Nicola, S. M., Surmeier, J., & Malenka, R. C. (2000). Dopaminergic modulation of neuronal
878 excitability in the striatum and nucleus accumbens. *Annual Review of Neuroscience*.
879 https://doi.org/10.1146/annurev.neuro.23.1.185

880 Oginsky, M. F., Goforth, P. B., Nobile, C. W., Lopez-Santiago, L. F., & Ferrario, C. R. (2016).
881 Eating "Junk-Food" Produces Rapid and Long-Lasting Increases in NAc CP-AMPA
882 Receptors: Implications for Enhanced Cue-Induced Motivation and Food Addiction.
883 *Neuropsychopharmacology*. https://doi.org/10.1038/npp.2016.111

884 Ouyang, J., Carcea, I., Schiavo, J. K., Jones, K. T., Rabinowitsch, A., Kolaric, R., … Carr, K.
885 D. (2017). Food restriction induces synaptic incorporation of calcium-permeable AMPA
886 receptors in nucleus accumbens. *European Journal of Neuroscience*.
887 https://doi.org/10.1111/ejn.13528

888 Paxinos, G and Franklin, K. B. J. (2012). Paxinos and Franklin's the Mouse Brain in
889 Stereotaxic Coordinates. In *São Paulo, Academic Press*.

890 Pennartz, C. M. A., Groenewegen, H. J., & Lopes da Silva, F. H. (1994). The nucleus
891 accumbens as a complex of functionally distinct neuronal ensembles: An integration of
892 behavioural, electrophysiological and anatomical data. *Progress in Neurobiology*.
893 https://doi.org/10.1016/0301-0082(94)90025-6

894 Petrovich, G. D. (2013). Forebrain networks and the control of feeding by environmental
895 learned cues. *Physiology and Behavior*, Vol. 121, pp. 10–18.

896 Roitman, M. F., Wheeler, R. A., Wightman, R. M., & Carelli, R. M. (2008). Real-time
897 chemical responses in the nucleus accumbens differentiate rewarding and aversive
898 stimuli. *Nature Neuroscience*. https://doi.org/10.1038/nn.2219

899 Rosenkranz, J. A., & Grace, A. A. (2002). Dopamine-mediated modulation of odour-evoked
900 amygdala potentials during pavlovian conditioning. *Nature*.
901 https://doi.org/10.1038/417282a

902 Sheng, M., & Greenberg, M. E. (1990). The regulation and function of c-fos and other
903 immediate early genes in the nervous system. *Neuron*. https://doi.org/10.1016/0896-
904 6273(90)90106-P

905 Shiflett, M. W., & Balleine, B. W. (2010). At the limbic-motor interface: Disconnection of
906 basolateral amygdala from nucleus accumbens core and shell reveals dissociable
907 components of incentive motivation. *European Journal of Neuroscience*.
908 https://doi.org/10.1111/j.1460-9568.2010.07439.x

909 Singer, B. F., Bubula, N., Li, D., Przybycien-Szymanska, M. M., Bindokas, V. P., & Vezina,
910 P. (2016). Drug-Paired Contextual Stimuli Increase Dendritic Spine Dynamics in Select
911 Nucleus Accumbens Neurons. *Neuropsychopharmacology*, *41*(8), 2178–2187.
912 https://doi.org/10.1038/npp.2016.39

913 Smith, R. J., Lobo, M. K., Spencer, S., & Kalivas, P. W. (2013). Cocaine-induced adaptations
914 in D1 and D2 accumbens projection neurons (a dichotomy not necessarily synonymous
915 with direct and indirect pathways). *Current Opinion in Neurobiology*.
916 https://doi.org/10.1016/j.conb.2013.01.026

917 Stefanelli, T., Bertollini, C., Lüscher, C., Muller, D., & Mendez, P. (2016). Hippocampal
918 Somatostatin Interneurons Control the Size of Neuronal Memory Ensembles. *Neuron*,
919 *89*(5), 1074–1085. https://doi.org/10.1016/j.neuron.2016.01.024

920 Strickland, J. A., Austen, J. M., & Sanderson, D. J. (2018). A biphasic reduction in a
921 measure of palatability following sucrose consumption in mice. *Physiology and*
922 *Behavior*. https://doi.org/10.1016/j.physbeh.2017.11.019

923 Struthers, W. M., DuPriest, A., & Runyan, J. (2005). Habituation reduces novelty-induced

924 FOS expression in the striatum and cingulate cortex. *Experimental Brain Research*.
925 https://doi.org/10.1007/s00221-005-0061-7

926 Stuber, G. D., Klanker, M., De Ridder, B., Bowers, M. S., Joosten, R. N., Feenstra, M. G., &
927 Bonci, A. (2008). Reward-predictive cues enhance excitatory synaptic strength onto
928 midbrain dopamine neurons. *Science*. https://doi.org/10.1126/science.1160873

929 Suto, N., Laque, A., De Ness, G. L., Wagner, G. E., Watry, D., Kerr, T., … Weiss, F. (2016).
930 Distinct memory engrams in the infralimbic cortex of rats control opposing
931 environmental actions on a learned behavior. *ELife*. https://doi.org/10.7554/eLife.21920

932 Taha, S. A. (2005). Encoding of Palatability and Appetitive Behaviors by Distinct Neuronal
933 Populations in the Nucleus Accumbens. *Journal of Neuroscience*.
934 https://doi.org/10.1523/JNEUROSCI.3975-04.2005

935 Taverna, S., Canciani, B., & Pennartz, C. M. A. (2005). Dopamine D1-Receptors Modulate
936 Lateral Inhibition Between Principal Cells of the Nucleus Accumbens. *Journal of*
937 *Neurophysiology*. https://doi.org/10.1152/jn.00672.2004

938 Te Morenga, L., Mallard, S., & Mann, J. (2013). Dietary sugars and body weight: systematic
939 review and meta-analyses of randomised controlled trials and cohort studies. *Bmj*.
940 https://doi.org/10.1136/bmj.e7492

941 Thompson, D. a, Moskowitz, H. R., & Campbell, R. G. (1976). Effects of body weight and
942 food intake on pleasantness ratings for a sweet stimulus. *Journal of Applied Physiology*.

943 Ting, J. T., Lee, B. R., Chong, P., Soler-Llavina, G., Cobbs, C., Koch, C., … Lein, E. (2018).
944 Preparation of Acute Brain Slices Using an Optimized N-Methyl-D-glucamine Protective
945 Recovery Method. *Journal of Visualized Experiments : JoVE*, (132).
946 https://doi.org/10.3791/53825

947 Tonegawa, S., Liu, X., Ramirez, S., & Redondo, R. (2015). Memory Engram Cells Have

948 Come of Age. *Neuron*, *87*(5), 918–931. https://doi.org/10.1016/j.neuron.2015.08.002

949 Tseng, K. Y., & O'Donnell, P. (2004). Dopamine-glutamate interactions controlling prefrontal
950 cortical pyramidal cell excitability involve multiple signaling mechanisms. *The Journal of*
951 *Neuroscience : The Official Journal of the Society for Neuroscience*, *24*(22), 5131–
952 5139. https://doi.org/10.1523/JNEUROSCI.1021-04.2004

953 Warren, B. L., Mendoza, M. P., Cruz, F. C., Leao, R. M., Caprioli, D., Rubio, F. J., … Hope,
954 B. T. (2016). Distinct Fos-Expressing Neuronal Ensembles in the Ventromedial
955 Prefrontal Cortex Mediate Food Reward and Extinction Memories. *Journal of*
956 *Neuroscience*. https://doi.org/10.1523/JNEUROSCI.0140-16.2016

957 West, E. A., & Carelli, R. M. (2016). Nucleus Accumbens Core and Shell Differentially
958 Encode Reward-Associated Cues after Reinforcer Devaluation. *Journal of*
959 *Neuroscience*. https://doi.org/10.1523/JNEUROSCI.2976-15.2016

960 Whitaker, L. R., Carneiro de Oliveira, P. E., McPherson, K. B., Fallon, R. V., Planeta, C. S.,
961 Bonci, A., & Hope, B. T. (2016). Associative Learning Drives the Formation of Silent
962 Synapses in Neuronal Ensembles of the Nucleus Accumbens. *Biological Psychiatry*.
963 https://doi.org/10.1016/j.biopsych.2015.08.006

964 Whitaker, L. R., & Hope, B. T. (2018). Chasing the addicted engram: identifying functional
965 alterations in Fos-expressing neuronal ensembles that mediate drug-related learned
966 behavior. *Learning & Memory (Cold Spring Harbor, N.Y.)*, *25*(9), 455–460.
967 https://doi.org/10.1101/lm.046698.117

968 Whitaker, L. R., Warren, B. L., Venniro, M., Harte, T. C., McPherson, K. B., Bossert, J. M., …
969 Hope, B. T. (2017). Bidirectional modulation of intrinsic excitability in rat prelimbic
970 cortex neuronal ensembles and non-ensembles following operant learning. *The Journal*
971 *of Neuroscience*. https://doi.org/10.1523/JNEUROSCI.3761-16.2017

972 Wilson, C. J. (2007). GABAergic inhibition in the neostriatum. *Progress in Brain Research*.

https://doi.org/10.1016/S0079-6123(06)60006-X

Yang, H., de Jong, J. W., Tak, Y. E., Peck, J., Bateup, H. S., & Lammel, S. (2018). Nucleus Accumbens Subnuclei Regulate Motivated Behavior via Direct Inhibition and Disinhibition of VTA Dopamine Subpopulations. *Neuron*. https://doi.org/10.1016/j.neuron.2017.12.022

Yawata, S., Yamaguchi, T., Danjo, T., Hikida, T., & Nakanishi, S. (2012). Pathway-specific control of reward learning and its flexibility via selective dopamine receptors in the nucleus accumbens. *Proceedings of the National Academy of Sciences of the United States of America*. https://doi.org/10.1073/pnas.1210797109

Ziminski, J. J., Hessler, S., Margetts-Smith, G., Sieburg, M. C., Crombag, H. S., & Koya, E. (2017). Changes in appetitive associative strength modulates nucleus accumbens, but not orbitofrontal cortex neuronal ensemble excitability. *Journal of Neuroscience*, *37*(12). https://doi.org/10.1523/JNEUROSCI.3766-16.2017

Ziminski, J. J., Sieburg, M. C., Margetts-Smith, G., Crombag, H. S., & Koya, E. (2018). Regional differences in striatal neuronal ensemble excitability following cocaine and extinction memory retrieval in Fos-GFP mice. *Neuropsychopharmacology*, *43*(4). https://doi.org/10.1038/npp.2017.101

996 **Figure legends**

997 Figure 1: Sucrose reward devaluation, but not caloric satiation, attenuates Pavlovian
998 approach behaviour. (A) Timeline for Pavlovian approach behavioural paradigm with
999 devaluation and caloric satiation. (B) Number of head entries in sucrose delivery magazine
1000 during acquisition in response to sucrose-associated cue (CS) are significantly higher than
1001 during intertrial interval (ITI), n = 32 asterisks indicate main effect of trial, ***p < 0.001. (C)
1002 Number of head entries during Pavlovian approach test in Non-devalued and Devalued
1003 mice. Head entries during the cue are significantly higher only in the Non-devalued
1004 condition. **p = 0.008, ***p < 0.001. n = 14-16 per group. (D) Body weight normalized to free
1005 feeding body weight in Non-devalued mice is significantly lower than in Devalued group. ***p
1006 < 0.001. n = 16 per group. (E) No difference in number of head entries during Pavlovian
1007 approach test during sucrose associated cue (CS) and intertrial interval (ITI) between *ad lib*
1008 chow and Control mice. Head entries during the cue are significantly higher. *p = 0.03, **p =
1009 0.007. n = 12 - 14 per group. (F) Body weight normalized to free feeding body weight in food
1010 restricted mice is significantly lower than in *ad lib* chow group independently of conditioning.
1011 ***p < 0.001. n = 12 - 14 per group. All values are mean ± SEM. Figure contributions: MCS,
1012 JJZ, GMS, HR, LSB performed experiments; MCS analysed the data

1013

1014 Figure 2: Fos expression in the Nucleus accumbens (NAc) shell. (A) Timeline for Pavlovian
1015 approach behavioural paradigm with devaluation and subsequent Fos analysis. (B) Reward-
1016 specific devaluation decreased the Fos expression. N = 14 per group, *p < 0.05. (C)
1017 Representative images of Fos staining in NAc shell in Non-devalued and Devalued groups.
1018 All values are mean ± SEM. Arrows indicate exemplary Fos positive cells, scale bar 100 µm,
1019 schematic overview modified after Paxinos and Franklin, 2001. Figure contributions: MCS
1020 performed experiments; MCS analyzed the data

1021

Figure 3: The increased excitability of GFP+ neurons compared to surrounding GFP– neurons in NAc shell is attenuated by reward devaluation. (A) Timeline for Pavlovian approach behavioural paradigm with devaluation. (B) Differential Interference Contrast (DIC) optics and confocal microscopy (GFP) were used to identify GFP+ (white arrow) and GFP– (red arrow) neurons, scale bar 20 µm. (C) In the Non-devalued group, GFP+ cells exhibit increased spiking in response to increasing current injections compared to surrounding GFP – cells. The I/V curve (inlay) for GFP+ cells are shifted in positive and negative current steps, but not in the intermediate range (GFP – *n* = 10/6, GFP + *n* = 11/6). Representative traces from injections at 116 pA (top). (C) After sucrose devaluation there is no difference in firing capacity between GFP+ and GFP– cells. Only a mild downward shift is observed for the I/V curves (inlay) from GFP+ and GFP – cells (GFP – *n* = 11/9, GFP + *n* = 11/8). Representative traces from injections at 116 pA (top). (D) GFP – cells exhibit an increased number of spikes after sucrose devaluation. (E) There is no difference in firing capacity or I/V curves (inlay) in GFP+ cells between Devalued and Non-devalued groups. *p < 0.05, **p < 0.01, ***p < 0.001. All values are mean ± SEM, values to the right of GFP− and GFP+ denote number of cells recorded/number of mice used, scale bar in representative traces 20 mV and 100 ms. Figure contributions: MCSperformed experiments; MCS, GMS analyzed the data

Figure 4: Basic passive membrane and action potential parameters in GFP+ and GFP– cells with and without devaluation. (A) RMP (resting membrane potential) was unchanged by devaluation or ensemble identity. (B) Rheobase was lower in GFP+ compared to GFP – cells without devaluation, **p = 0.0047, (Non-devalued: GFP – *n* = 9/5, GFP + *n* = 10/6, Devalued: GFP – *n* = 11/9, GFP + *n* = 10/8) (C) Input resistance was specifically increased in GFP+ cells without devaluation, **p 0.0021, (Non-devalued: GFP – *n* = 10/6, GFP + *n* = 10/6, Devalued: GFP – *n* = 11/9, GFP + *n* = 10/8) (D) AP half-width was specifically increased in Non-devalued GFP+ neurons, *p = 0.0103, **p = 0.0052. (Non-devalued: GFP

– *n* = 10/6, GFP + *n* = 11/6, Devalued: GFP – *n* = 10/9, GFP + *n* = 10/8) (E) AHP (Afterhyperpolarisation) was unchanged by devaluation or ensemble identity. (F) AP amplitude was unchanged by devaluation or ensemble identity. All values are means ± SEM, values to the right of GFP− and GFP+ denote number of cells recorded/number of mice used, asterisks indicate post-hoc comparisons after two-way ANOVAs. Figure contributions: MCS, JJZ performed experiments; MCS analyzed the data

Figure 5: Devaluation did not modulate the synaptic strength of GFP+ neurons. (A) AMPAR/NMDAR ratios between GFP+ and GFP– neurons were similar in both Non-devalued and Devalued groups (Non-devalued GFP– 7/7, GFP+ 6/5; Devaluation GFP– 6/6, GFP+ 4/3). Above: Representative AMPAR/NMDAR traces from GFP+ and GFP– neurons. Scale bar 50 pA, 50 ms. (B) AMPAR rectification was similar in activated ensembles following Non-devaluation and devaluation (Non-devalued GFP– 5/4, GFP+ 4/4; Devalued GFP– 5/4, GFP+ 5/3). Data shown are normalized to the current peak at -80 mV. Right: representative images of Non-devalued and Devalued rectification curves in GFP+ and GFP– neurons at +40 mV (grey) and -80 mV (black). Scale bar 50 pA, 10 ms. (C) Representative sEPSC traces from Non-devalued and Devalued mice. Scale bar 20 pA, 100 ms. Spontaneous excitatory post-synaptic potential (sEPSC) frequency (left) and amplitude (right) were not selectively modulated in GFP+ and GFP– neurons (Non-devalued GFP– 19/8, GFP+ 15/8; Devalued GFP– 17/6, GFP+ 18/6). However, reward devaluation reduced sEPSC frequency non-selectively across both neuron types (* $p < 0.05$). (D) Paired pulse ratios were similar in GFP+ and GFP– neurons from Non-devalued and Devalued mice (Non-devalued GFP– 13/10, GFP+ 8/8; Devalued GFP– 8/7, GFP+ 5/4). Scale bar 100 pA, 10ms. Data are expressed as mean ± SEM; values to the right of GFP− and GFP+ denote number of cells recorded/number of mice used. Figure contributions: JJZ, MCS performed experiments; JJZ analyzed the data

Table legends

Table 1: Data in first four columns are expressed as mean ± SEM. *p < 0.05, **p < 0.01 post-hoc comparison GFP+ vs GFP–. ^p < 0.05 post-hoc comparison non devalued vs devalued, RMP = resting membrane potential, AHP = afterhyperpolarisation

Table 2: Summary of statistical analyses

Figure 1

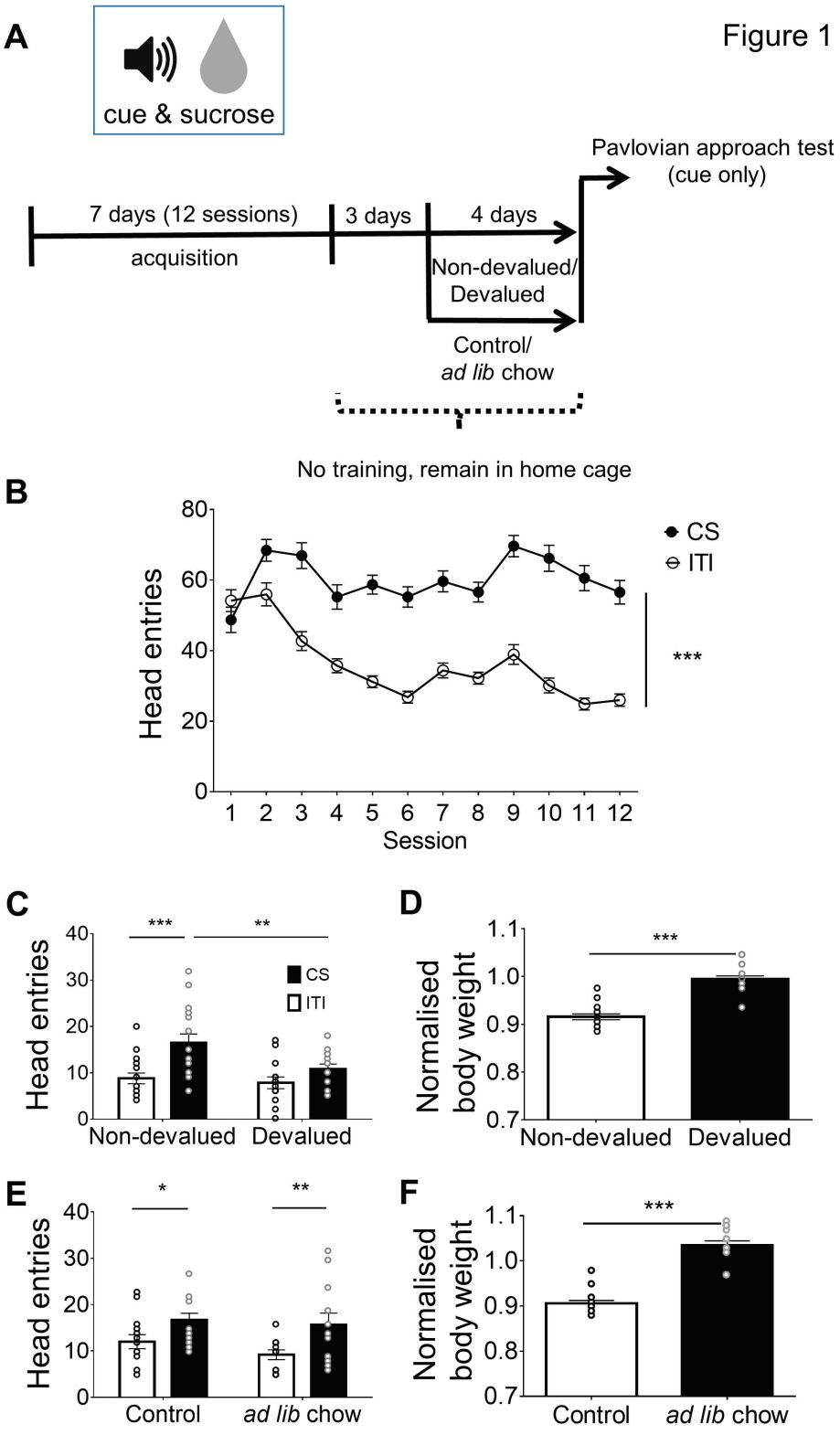

Figure 2

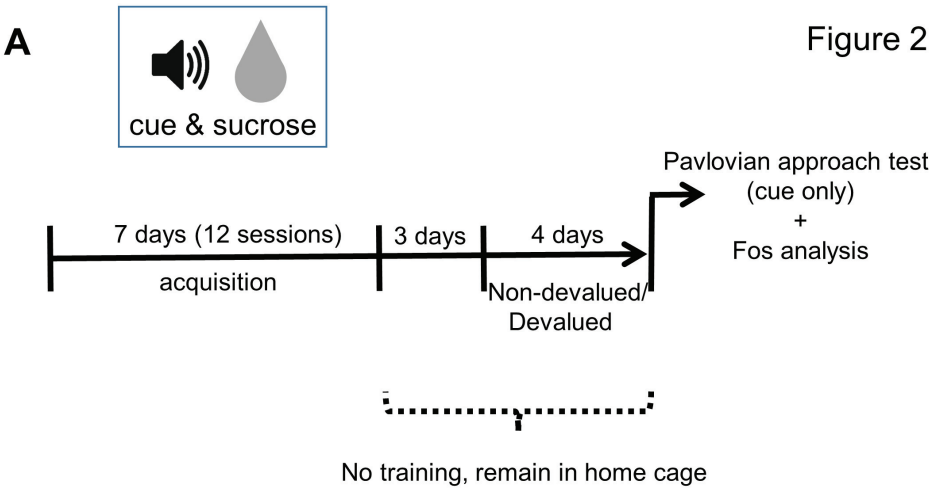

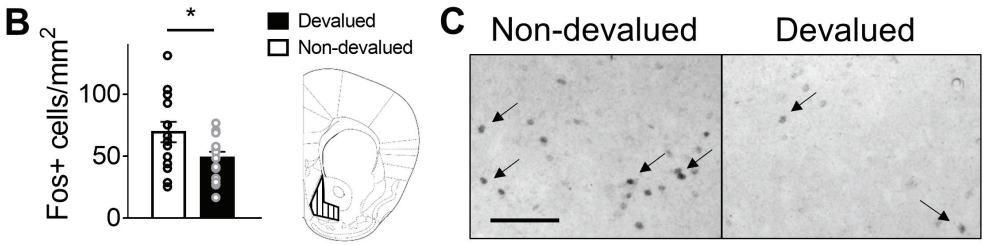

Figure 3

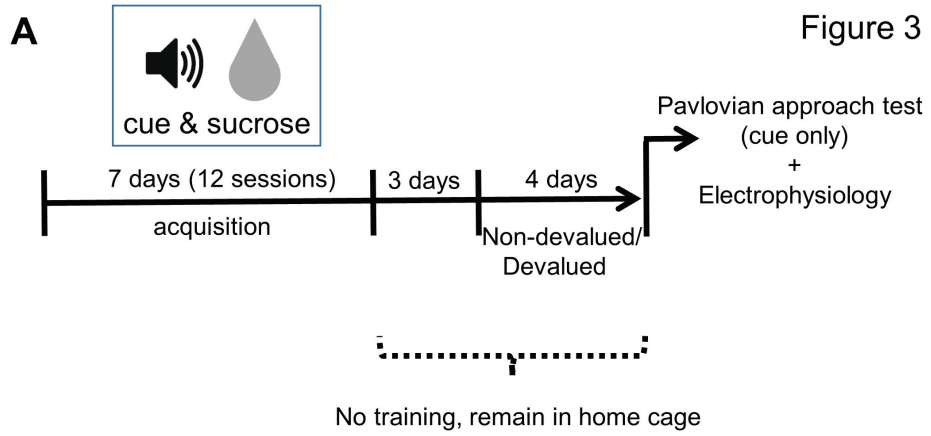

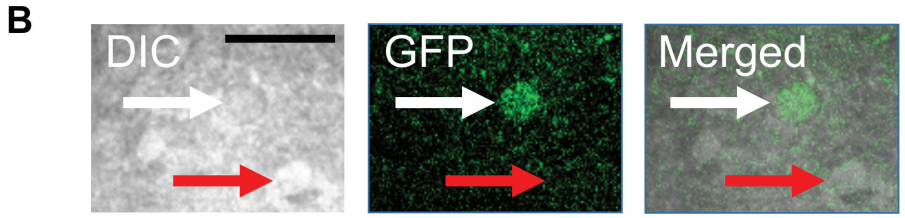

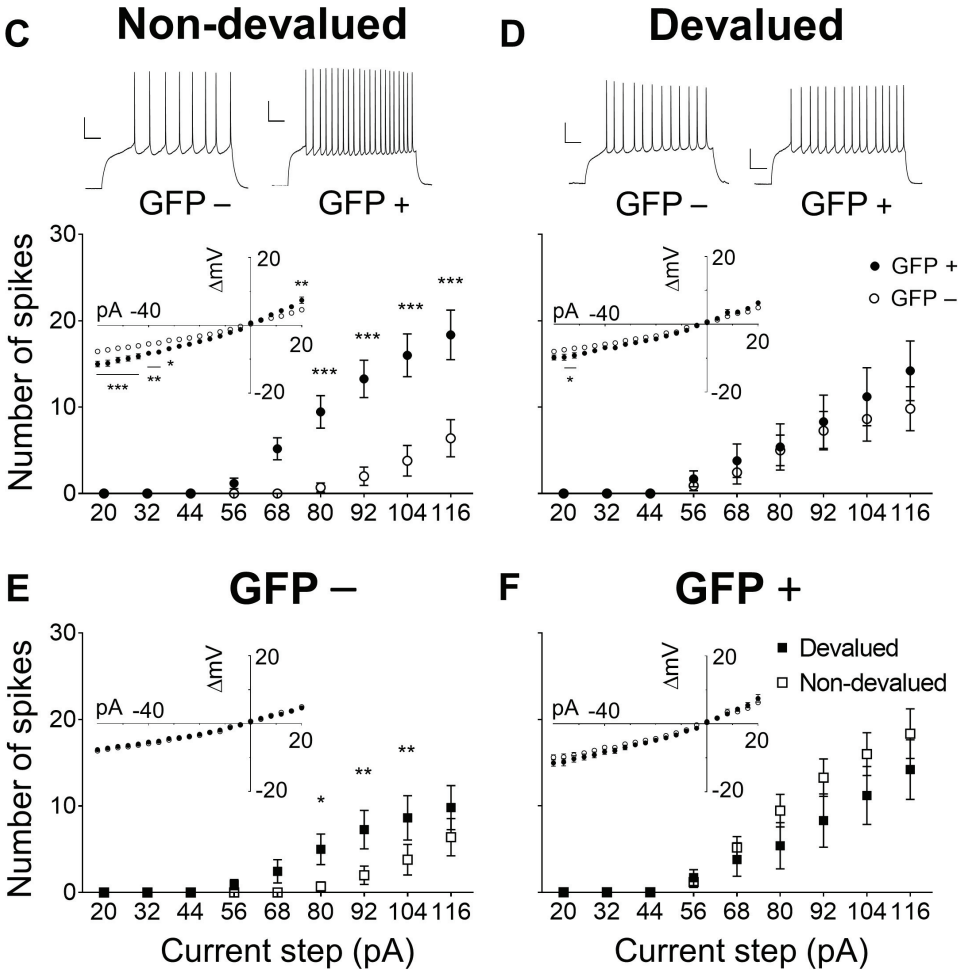

Figure 4

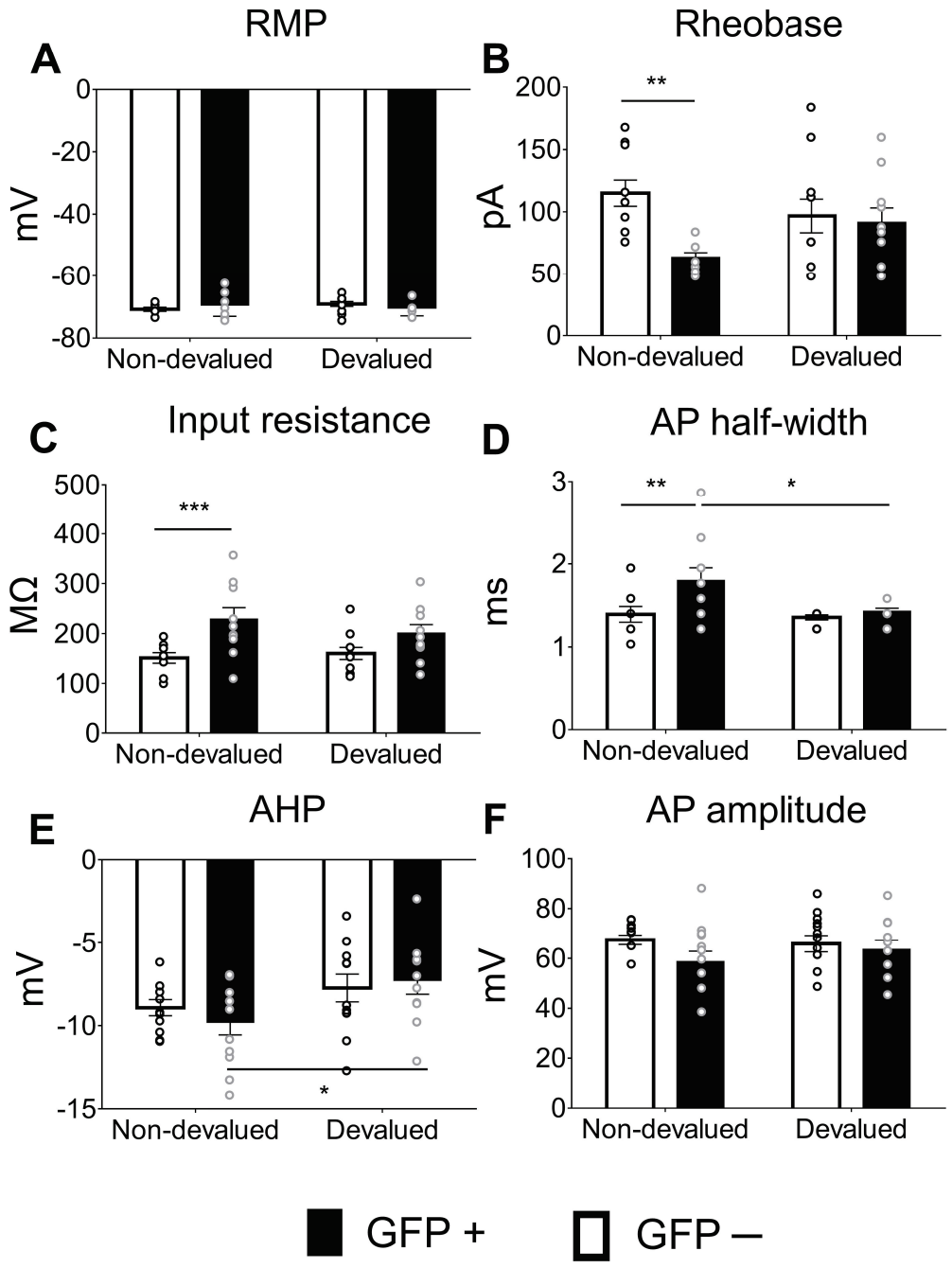

Figure 5

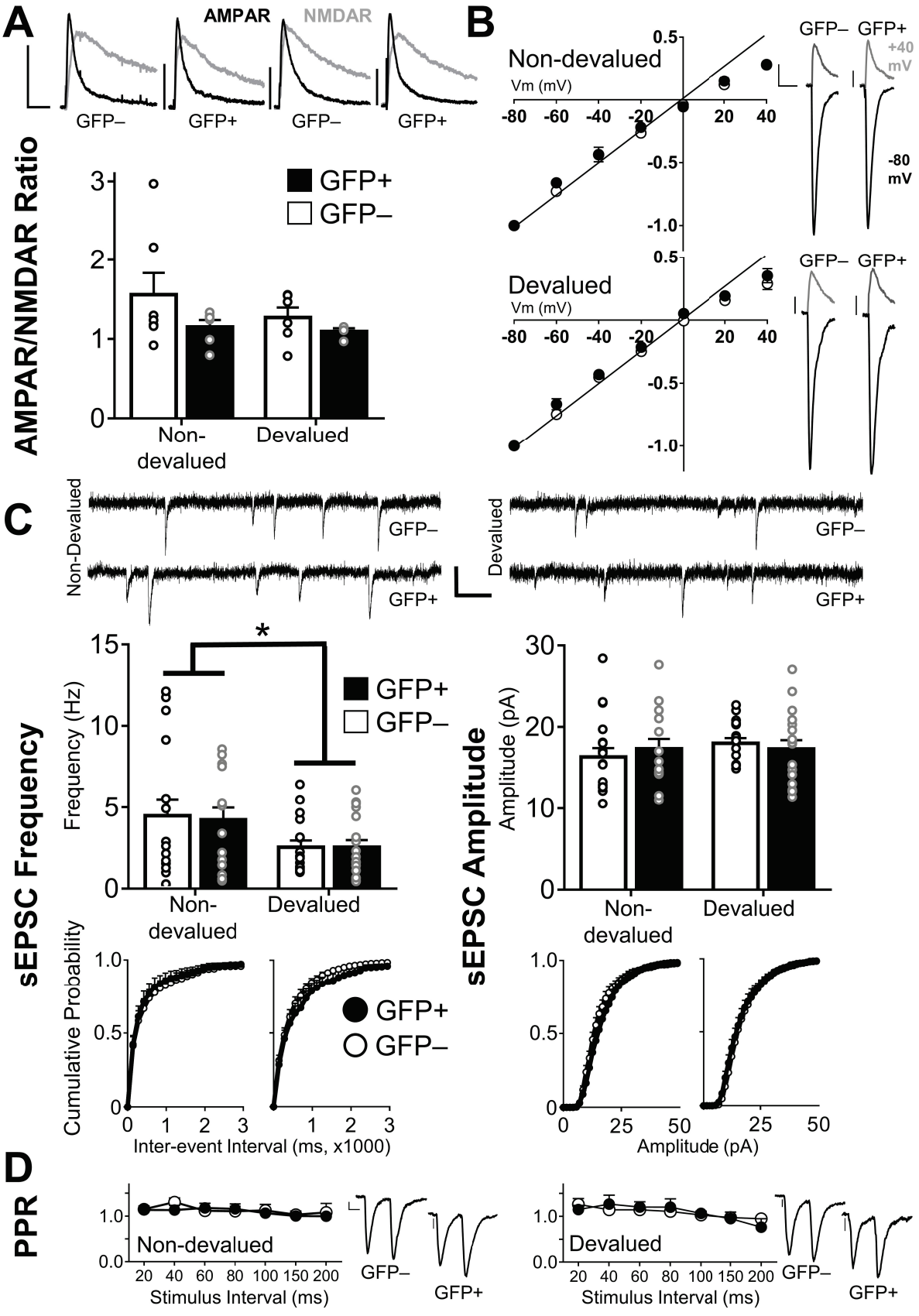

Table 1: Basic membrane properties from the NAc shell in Non-devalued and Devalued mice

	Non-devalued		Devalued		Interaction	Main effect	
	GFP -	GFP +	GFP -	GFP +	GFP x Devaluation	GFP	Devaluation
RMP (mV)	-70.8 ± 0.7	-69.4 ± 1.1	-69.1 ± 0.8	-70.3 ± 0.8	F(1,38)=2.28, p=0.14	F(1,38)=0.19, p=0.66	F(1,38)=0.02, p=0.9
Rheobase (pA)	115.0 ± 10.5**	63.2 ± 4.0**	96.7 ± 13.5	91.2 ± 11.9	F(1,37)=4.57, p=0.04	F(1,37)=0.20, p=0.66	F(1,37)=7.02, p=0.01
Input resistance (MΩ)	151.2 ± 10.7***	246.5 ± 27.6***	160.2 ± 12.0	200.6 ± 17.2	F(1,37)=1.28, p=0.26	F(1,37)=13.04, p<0.01	F(1,37)=0.34, p=0.57
AHP (mV)	-8.9 ± 0.5	-9.8 ± 0.8^	-7.7 ± 0.8	-7.3 ± 0.8^	F(1,38)=0.78, p=0.38	F(1,38)=0.07, p=0.79	F(1,38)=6.07, p=0.02
AP half-width (ms)	1.4 ± 0.1**	1.8 ± 0.15**^	1.4 ± 0.03	1.4 ± 0.04^	F(1,37)=2.9, p=0.1	F(1,37)=6.0, p=0.02	F(1,37)=4.31, p=0.04
AP amplitude (mV)	67.4 ± 1.9	58.7 ± 4.2	65.9 ± 3.3	63.5 ± 3.8	F(1,37)=0.82, p=0.37	F(1,37)=2.53, p=0.12	F(1,37)=0.22, p=0.64

	Data structure	Type of test	Confidence interval 95%												
Check for pre-existing differences in acquisition of Pavlovian conditioning between (future) groups: Devalued vs. Non-devalued and *ad lib* chow vs. control	Quantification of head entries during acquisition of Pavlovian conditioning during CS and ITI, displayed as difference score.	Two-way mixed ANOVAs	session	1	2	3	4	5	6	7	8	9	10	11	12
			Non-devalued	0.14-0.02	0.0069 - 0.16	0.18 - 0.30	0.15 - 0.33	0.24 - 0.40	0.28 - 0.40	0.19 - 0.35	0.21 - 0.35	0.22 - 0.38	0.29 - 0.41	0.34 - 0.44	0.30 - 0.46
			Devalued	-0.25 - 0.055	0.014 - 0.29	0.13 - 0.27	0.033 - 0.25	0.25 - 0.39	0.29 - 0.45	0.18 - 0.32	0.17 - 0.35	0.21 - 0.39	0.31 - 0.49	0.41 - 0.51	0.25 - 0.41
			control	-0.28 - 0.059	-0.0060 - 0.21	0.057 - 0.26	0.0019 - 0.22	0.074 - 0.25	0.053 - 0.27	0.14 - 0.38	0.18 - 0.40	0.24 - 0.32	0.13 - 0.25	0.21 - 0.35	0.23 - 0.37
			Ad lib chow	-0.066 - 0.088	0.030 - 0.19	0.22 - 0.34	0.044 - 0.28	0.11 - 0.25	0.20 - 0.34	0.16 - 0.34	0.18 - 0.34	0.19 - 0.33	0.17 - 0.35	0.23 - 0.35	0.11 - 0.35
Acquisition of Pavlovian conditioning (Figure 1B)	Quantification of head entries during acquisition of Pavlovian conditioning during CS and ITI.	Two-way repeated measures ANOVA	session	1	2	3	4	5	6	7	8	9	10	11	12
			CS	41.34 - 56.04	62.12 - 74.76	58.39 - 72.25	48.13 - 62.31	53.28 - 64.16	49.29 - 61.15	55.64 - 66.48	50.85 - 62.33	65.36 - 76.70	59.76 - 71.30	53.28 - 67.84	49.93 - 59.59
			ITI	46.08 - 56.86	50.13 - 61.81	37.22 - 48.16	31.68 - 39.76	27.73 - 34.59	23.32 - 30.24	29.49 - 37.29	28.78 - 35.60	33.18 - 44.58	25.32 - 32.56	20.90 -27.16	22.41 - 29.53
Pavlovian approach test (Figure 1C, E)	Quantification of head entries during Pavlovian approach test during CS and ITI in Devalued vs. Non-devalued and *ad lib* chow vs. control groups.	Two-way mixed ANOVAs		CS	ITI										
			Non-devalued	12.28 - 20.60	6.35 - 11.27										
			Devalued	8.61 - 13.11	5.20 - 8.80										
			control	13.68 - 19.74	8.73 - 15.27										
			Ad lib chow	9.90 - 21.26	6.84 - 11.50										
Body weights (Figure 1D, F)	Body weights normalized to free feeding body weight in Devalued vs. Non-devalued and *ad lib* chow vs. control groups.	Unpaired two-tailed t-tests	Non-devalued	0.91 - 0.93											
			Devalued	0.99 - 1.01											
			control	0.89 - 0.91											
			Ad lib chow	1.01 - 1.05											

Fos quantification (Figure 2B)	Quantification of Fos+ cells in NAc shell in Devalued and Non-devalued groups. Two images were taken per hemisphere (dorsal and ventral) and numbers of Fos+ neurons were added to get one value per hemisphere, between hemispheres values were averaged to get one value per mouse.	Two-tailed t-test	Non-devalued	58.01 - 98.83
			Devalued	39.83 - 64.97

Excitability data (Figure 3C, D, E, F)	Quantification of action potentials after injection of increasing current steps (20pA – 116pA) in GFP+ and GFP– neurons in Devalued and Non-devalued groups.	Three-way mixed ANOVAs, Two-way mixed ANOVAs		current step (pA)	20	32	44	56	68	80	92	104	116	
			Non-devalued	GFP–	0.0 - 0.0	0.0 - 0.0	0.0 - 0.0	0.0 - 0.0	0.0 - 0.0	0.0 - 0.0	-0.41 - 4.41	-0.20 - 7.80	1.53 - 11.27	
				GFP+	0.0 - 0.0	0.0 - 0.0	0.0 - 0.0	-0.21 - 0.87	2.35 - 8.01	5.25 - 13.65	8.42 - 18.12	10.48 - 21.52	11.95 - 24.77	
			Devalued	GFP–	0.0 - 0.0	0.0 - 0.0	0.0 - 0.0	-0.15 - 0.37	-0.71 - 3.51	1.07 - 8.93	2.32 - 12.22	2.92 - 14.36	4.16 - 15.48	
				GFP+	0.0 - 0.0	0.0 - 0.0	0.0 - 0.0	-0.38 - 3.78	-0.59 - 8.19	-0.66 - 11.46	1.32 - 15.28	3.62 - 18.78	6.38 - 22.02	

I/V curves (inlays Figure 3C, D, E, F)	Voltage displacement (mV) to subthreshold current injections in the range of (-60pA – 20 pA) in GFP+ and GFP– neurons in Devalued and Non-devalued groups.	Three-way mixed ANOVAs, Two-way mixed ANOVAs			-60	-56	-52	-48	-44	-40	-36	-32	-28	-24	-20	-16	-12	-8	-4	0	4	8	12	16	20
			Non-devalued	GFP–	-8.59 - -4.92	-8.39 - - 6.02	-7.82 - -5.62	-7.52 - - 5.35	-7.01 - - 5.04	- 6.40 - - 4.50	- 6.03 - - 4.32	-5.21 - - 3.61	- 4.89 - - 3.34	- 4.36 - - 3.03	-3.84 - - 2.48	- 3.84 - - 2.48	- 2.30 - - 1.50	- 1.49 - - 0.99	-0.83 - - 0.49	- 0.049 - 0.61	1.08 - 1.70	1.58 - 2.71	2.21 - 3.28	2.90 - 4.39	3.80 - 5.37
				GFP+	-13.6 - -9.3	-13.6 - -8.8	-12.4 - -8.1	-11.7 - -7.6	-11.0 - - 7.1	-9.9 - - 6.4	- 9.60 - - 6.14	-8.47 - - 5.32	- 7.47 - - 4.80	- 6.95 - - 4.17	-6.13 - - 3.47	- 5.18 - - 2.95	- 4.11 - - 2.37	- 2.73 - - 1.49	-1.80 - - 0.40	-0.30 - - 1.18	1.11 - 2.13	1.89 - 4.02	3.004 - 4.56	3.61- 6.26	4.95 - 10.081
			Devalued	GFP–	-8.45 - -6.88	- 7.90- -6.31	-7.48 - -5.97	-7.78 - - 5.85	-7.31 - - 5.37	- 6.46 - - 4.73	- 5.70 - - 4.54	-5.69 - - 3.96	- 4.60 - - 3.54	- 4.10 - - 3.19	-3.56 - - 2.85	- 2.73 - - 2.08	- 2.81 - - 1.82	- 1.42 - - 0.99	-1.18 - - 0.22	-0.32 - 0.70	0.88 - 1.92	1.96 - 2.53	2.46 - 4.09	2.66 - 4.09	3.66 - 5.12
				GFP+	- 11.510 - -8.13	- 11.75 - - 7.70	- 11.056 - -7.33	- 1.005 - - 7.058	- 9.102 - - 6.49	- 8.09 - - 5.73	- 8.28 - - 5.59	- 7.088 - - 4.76	- 6.53 - - 4.28	- 5.29 - - 3.53	- 4.52- -3.18	- 4.25 - - 2.67	- 3.18 - - 2.12	- 1.72 - - 1.21	- 1.056 - 0.46	-0.16 - 1.10	1.07 - 1.75	1.87 - 3.52	2.71 – 4.50	3.79 – 5.54	4.90 – 7.73

Membrane and AP parameters (Figure 4A – F, Table 1)	RMP, input resistance, AHP, AP amplitude and half-width, Rheobase in GFP+ and GFP– neurons in Devalued and Non-devalued groups.	Two-way ANOVAs	RMP	Non-devalued	GFP–	-72.30 - -69.30
					GFP+	-71.82 - -66.90
				Devalued	GFP–	-70.88 - -67.30
					GFP+	-72.15 - -68.45
			Input resistance	Non-devalued	GFP–	127.02 - 175.28
					GFP+	185.04 - 308.02
				Devalued	GFP–	131.78 - 170.12
					GFP+	161.81 - 239.41
			AHP	Non-devalued	GFP–	-10.02 - -7.82
					GFP+	-11.49 - -8.09
				Devalued	GFP–	-9.60 - -5.88
					GFP+	-9.18 - -5.38
			AP amplitude	Non-devalued	GFP–	67.83 - 72.03
					GFP+	49.43 - 67.99
				Devalued	GFP–	58.67 - 73.17
					GFP+	54.98 - 72.08
			AP half-width	Non-devalued	GFP–	1.17 - 1.61
					GFP+	1.42 - 1.94
				Devalued	GFP–	1.29 - 1.43
					GFP+	1.35 -1.51
			rheobase	Non-devalued	GFP–	91.26 - 138.74
					GFP+	54.17 - 72.23
				Devalued	GFP–	61.02 -120.98
					GFP+	64.20 - 118.20

AMPAR/NMDAR current ratio (Figure 5A)	Ratios of AMPAR to NMDAR currents (recorded at +40 mV) in GFP+ and GFP– neurons in Devalued and Non-devalued groups.	Two-way ANOVAs	Non-devalued	GFP–	0.88 - 2.24
				GFP+	0.93 - 1.37
			Devalued	GFP–	0.95 - 1.59
				GFP+	0.95 - 1.23
AMPAR rectification index (Figure 5B)	Absolute ratios of AMAR EPSC recorded at -80 mV to the EPSC recorded at +40 mV in GFP+ and GFP– neurons in Devalued and Non-devalued groups.	Two-way ANOVA	Non-devalued	GFP–	2.91 - 4.43
				GFP+	3.11 - 3.97
			Devalued	GFP–	1.88 - 5.98
				GFP+	1.65 - 4.73
Chord Conductance Ratios	Chord Conductance (G=I/V) at +40 mV was divided by the chord conductance at -80 mV in GFP+ and GFP– neurons in Devalued and Non-devalued groups.		Non-devalued	GFP–	0.44 - 0.68
				GFP+	0.50 - 0.64
			Devalued	GFP–	0.32 - 0.84
				GFP+	0.39 - 1.01
sEPSC Frequency (Figure 5C)	Number of sEPSCs over a 30 second period expressed in Hz in GFP+ and GFP– neurons in Devalued and Non-devalued groups.	Two-way ANOVA	Non-devalued	GFP–	2.37 - 6.59
				GFP+	2.63 - 5.83
			Devalued	GFP–	1.66 - 3.42
				GFP+	1.60 - 3.48
sEPSC Amplitude (Figure 5C)	Mean amplitude of sEPSCs over a 30 second period expressed in Hz in GFP+ and GFP– neurons in Devalued and Non-devalued	Two-way ANOVA	Non-devalued	GFP–	14.05 - 18.59
				GFP+	14.77 - 19.91
			Devalued	GFP–	16.73 - 19.31
				GFP+	15.07 - 19.57

	groups.										
Paired Pulse Ratios (Figure 5D)	Ratio of second to first evoked EPSC over inter-stimulus intervals of 20, 40, 60, 80, 100, 150 and 200 ms in GFP+ and GFP– neurons in Devalued and Non-devalued groups.	Three-way mixed ANOVA		ISI	20	40	60	80	100	150	200
			Non-devalued	GFP–	1.01 - 1.29	1.11 - 1.51	0.96 - 1.28	0.86 - 1.34	0.83 - 1.41	0.86 - 1.20	0.65 - 1.51
				GFP+	0.92 - 1.34	0.89 - 1.37	0.94 - 1.42	0.90 - 1.42	0.93 - 1.19	0.89 - 1.11	0.90 - 1.10
			Devalued	GFP–	0.96 - 1.56	0.92 - 1.36	0.93 - 1.35	0.93 - 1.29	0.84 -1.22	0.88 - 1.06	0.84 - 1.06
				GFP+	0.90 - 1.40	0.73 - 1.81	0.88 - 1.52	0.70 - 1.70	0.93 - 1.19	0.56 - 1.34	0.25 - 1.27

Table 2: Summary of statistical analyses